Surface Patterned Ceramics Via Breath Figures Method With Potential Application As Implant Coatings

Cristiano Carlomagno

October 2018

SURFACE PATTERNED CERAMICS VIA BREATH FIGURES METHOD WITH POTENTIAL APPLICATION AS IMPLANT COATINGS

Cristiano Carlomagno

E-mail: cristiano.carlomagno@unitn.it

Approved by:

Prof. Claudio Migliaresi
Department of Industrial Engineering
University of Trento, Italy

Prof. Devid Maniglio
Department of Industrial Engineering
University of Trento, Italy

Ph.D. Commission:

Prof Vamsi K. Yadavalli
Department of Chemical and Life Science
Virginia Commonwealth University, USA

Prof. Yifu Ding
Department of Mechanical Engineering
University of Colorado at Boulder*, USA*

Prof. Gian Domenico Sorarù
Department of Industrial Engineering
University of Trento, Italy

University of Trento
Department of Industrial Engineering

October 2018

Abstract

Surface porous silicon based ceramics are a class of materials with excellent mechanical, physical and chemical properties and for this reason they are widely used in different fields of application. The resultant properties of these material are due principally to the combination of the chemical composition (coordination with the Si atom) and the specific geometry of the pattern. These parameters are able to influence phenomena such as the biological activity, the exposed surface area and the thermal, mechanical and chemical resistance. Techniques used nowadays to synthesize these ceramics with a specific patter are usually really complicated, expensive and time-consuming with limitations for the large-scale industrial application. The Breath Figure method is a new fast and highly controllable technique that allows to decorate the surface of polymer films with different porous patterns. A large variety of starting materials can be used to perform this process, obtaining porous films with different characteristics and with a specific control on the entire process. In this work we used a UV cross-linkable polysiloxane as precursor for the Breath Figure process in order to combine the pattern procedure with the polymer derived ceramic method. Initially, the effects of the process variables on the final surface porosity was evaluated, identifying the parameters which most influence the final material. After the patterning, materials with different characteristics were pyrolyzed under different atmospheres in order to induce simultaneously the ceramic conversion and the chemical modification of the silicone structure. Three different porous silicon-based ceramics were obtained using flowing air, nitrogen and ammonia during the heat treatments, respectively: silicon dioxide, silicon oxycarbide and silicon oxynitride. All these material have been proposed as implant coating for different body districts, but recent studies demonstrated the potential application of silicon oxynitrides as bone implant coatings due to the enhanced bioactivity and osteoinductivity of the ceramic. For this reason in the second part of this work we evaluated the potential bioactivity of surface porous silicon oxynitrides in terms of bioactive silicon ions release capability and effects of different porosity degrees on cells behavior. Four different surface pattern were applied on titanium alloy disks and used for an *in vitro* characterization using human Mesenchymal Stem Cells and compared with uncoated titanium. The results indicated that the silicon ions release from the coating surface leads to an increase of the cellular activity with the porous pattern influencing the hMSC initial adhesion and proliferation.

...to my Nonna,
to my Father and to my Mother...

PhD Thesis:

Surface patterned ceramics via Breath Figures method with potential applications as implant coatings

Cristiano Carlomagno

E-mail: cristiano.carlomagno@unitn.it

Supervisors:

Prof. Claudio Migliaresi

Department of Industrial Engineering

University of Trento

Dr. Devid Maniglio

Department of Industrial Engineering

University of Trento

Introduction

Experimental Section

Bibliography

Academic Events

Acknowledgments

Introduction

1.   Patterned polymer derived ceramics

1.1.   Introduction

In the last 30 years, the fabrication of mainly Si-based ceramics starting from polymer precursors has been denoted as Polymer Derived Ceramics (PDCs). The process facility and the unique features of the derived materials contributed to the large employment of these materials in many fields of application. PDCs represent a process in which a polymer, usually in a soluble form, is converted in the corresponding ceramic material through a heat treatment between 400 and 2000°C in a controlled atmosphere [1]. The precursor with a specific chemical composition represents the inorganic or organic complex from which the resultant ceramic material is tailored both for chemical composition and micro/nano structure. PDCs are interesting for the fast and easy process that leads to the formation of a totally additive-free ceramic material with high temperature tolerance (up to 2000°C) and good oxidative and creep resistance [2]. Generally, polymer solutions are exposed to a cross-linking process in order to "freeze" the structure. During this step, polymer solutions can be shaped into specific forms using different techniques. This allows expanding the potential final applications, for example by increasing the ceramic surface area through an imprinting of nano/micro structure [3]. The consecutive heat treatment under a specific atmosphere have two main effects: it drives the ceramic conversion and it induces chemical modifications with the inclusion or the removal of specific chemical groups. These two phenomena are possible thanks to the polymer nature of the starting material, whose chemical structure, while transforming into ceramic, can be reorganized and modified through the pyrolysis treatment.

1.2. Preceramic Polymers

The molecular composition of the polymer used as preceramic material, influences not only the final chemical composition but also the final phases distribution and nano/micro structure. An example is given by some silicon containing PDCs (silicon carbonitrides, SiCN, and silicon oxycarbides, SiOC) in which the strong bonding between silicon and carbon in the preceramic polymer prevents the removal of carbon under inert atmospheres. Using oxidative atmospheres instead of the inert one, different chemical modifications can be performed, for example coordinating nitrogen groups into the Si-O network and removing carbon groups, resulting in the final silicon oxynitride (SiON) [4]. In figure 1 a simplified formula of the organosilicon polymer suitable for the PDCs process is represented. The R^1, R^2 and X groups influence different final ceramic properties such as chemical and thermal stability, polymer solubility and electronic, optical and rheological properties [2]. For example, different X groups result in various Si-based polymers including polyorganosilanes (X=Si), polyorganocarbosilanes (X=CH$_2$), polyorganosiloxanes or silicones (X=O), polyorganosilazanes (X=NH) and polyorgnosilylcarbodiimides (X=N=C=N). In the same way, also R^1 and R^2 groups can influence the same properties. Usually hydrogen, aliphatic or aromatic groups are attached to the R chain controlling the overall carbon content both in the preceramic polymer and in the final ceramic structure. The nature of the R groups has an important influence on solubility, thermal stability, viscosity and cross-linking of the starting polymer, driving also the ceramic conversion mechanism [5].
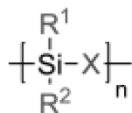
$$\left[\begin{array}{c} R^1 \\ | \\ Si-X \\ | \\ R^2 \end{array}\right]_n$$

Figure 1 Schematic representation of silicon-based precursors. Adapted from [2]

The main preceramic polymer characteristics, to be efficient during the conversion process, are the sufficient molecular weight to avoid the volatilization of the compound with a low molecular weight; the optimal solubility in organic solvents to be effective during the shaping process and the high reactivity when a chemical or physical cross-linking is induced [2]. The main silicon-based preceramic polymers used in PDCs are poly (organosilanes), poly (organocarbosialnes), poly (organosilazanes), poly (organosilylcarbodiimides) and poly (organosiloxanes). *Poly(organosilanes)* are based on the Si-Si backbone with organic groups coordinated with the silicon atoms. Their importance is due to the intrinsic photo-conductivity, luminescence and thermal stability [2,6]. For these properties, polysilanes have found application in photo resists, hole-transporting, semi-conductors and silicon-carbide based ceramics in PDCs route. *Poly(organocarbosilanes)* are complex and hyper branched materials based on Si-C and Si-Si backbone. Common R groups coordinated with the principal structure are phenylene, ethylene and sil(an)ylene that ensure a high ceramic yield in the corresponding Si-C-based material [7]. The most interesting ceramic material produced from polycarbosilanes are the Si-C based fibers due to their high mechanical and chemical properties [8]. *Poly(organosilazanes)* are polymers used nowadays as sylylating agents in chemistry processes and as single source precursors for PDCs by pyrolysis. The main advantage of these materials is the high ceramic yield for the synthesis of SiN used in dielectrics, anti-corrosion and high temperature applications. The main limitation in the usage of polysilazanes is the low molecular weight and cross-linking rate of the starting material, which needs further chemical modifications to be used as precursor in PDCs [2]. *Poly(organosilylcarbodiimides)* is the second class of precursor that, after thermal decomposition and reorganization, lead to the formation of N containing Si-based ceramics. The resultant ceramic presents a higher thermal stability if compared with the precursors described above, presenting at the same time a higher molecular weight and cross-linking rate due to the high carbon content [9]. The most promising material in PDCs field

3

is represented by *Poly(organosiloxanes)* also called silicones. These materials are widely used as buildings and/or biomedical sealants due to the excellent electrical, chemical and physical properties and also for the great variety of products commercially available. Silicones present a Si-O-Si base composition, with the R groups enriched with carbon moieties both to increase the mechanical and chemical properties of the material and also to induce a strong chemical and/or physical cross-linking [2]. R groups are often represented by methyl, ethyl, propyl, phenyl, vinyl, fluoroalkyl or alkoxy groups. These polymers are also widely used in the pharmaceutical and biomedical field where are used in direct contact with the human body as skin adhesive patches, tooth root sealer, electrical and pressure sensitives adhesive sensors, drug delivery systems, skin emollients, contact lenses and surgery implants [10]. The silicone cross-linking is fundamental for several reasons, but principally to increase mechanical properties and chemical resistance making at the same time the material insoluble and heat treatable. The general mechanism for chemical or physical (e.g. UV-exposition) cure, involves the reaction of Si-H side groups with vinyl species ($CH=CH_2$), which contains in the case of the chemical cure, also specific catalysts [11]. The curing process, besides the increase in material properties, leads also to the formation of a nano/micro random porosity due to the large Si atomic volume and also to the high flexibility of the Si-H bond. This "empty volume" is exploited in the biomedical field to upload drugs used in drug delivery systems.

1.3.   Ceramic conversion

Starting from the different silicon-based polymers described in previous paragraph, after the thermal treatment at around 1000°C, silicon-based amorphous ceramic PDCs can be obtained. The ceramic conversion involves the decomposition and/or elimination and reorganization of organic species, including methyl, phenyl, vinyl groups, and of silicon coordination, such as Si-H, Si-OH, Si-C and Si-NH$_x$. The heat treatment is usually conducted in

oven using specific oxidative or inert gas atmospheres. Using inert atmospheres (e.g. Nitrogen or Argon) the elimination through combustion of organic species is induced with the reorganization of the Si-X backbone, while, using oxidative atmospheres (e.g. Ammonia and Oxygen) the introduction of new groups through nitridation or the complete removal of carbon-containing moieties can be catalyzed [2]. Different process parameters can affect the final ceramic, including: preceramic polymer characteristics, filler presence, atmosphere type and pressure, heating rate and temperature and dwelling time. one example is given by the flowing gas pressure, which is able to avoid the carbothermal reduction at high temperature and pressures, while, the process under vacuum promotes it. The heating rate largely affects ceramic yield and chemical composition due to the different energy transfer and consequent effects on oligomers. Parameters related with the sample exposition to high temperatures, such as heating rate, dwelling time and temperature, influence also the homogeneity of the final ceramic. It has been demonstrated that low heating rate (e.g. 2-5°C/min) are able to prevent cracks formation due to the release caused by the gas release during the process [2,12,13]. As explained before, the process atmosphere is a fundamental parameter that have influence on the final ceramic chemical composition. In the last decades, this phenomena was intensively investigated regarding the possibility to obtain different ceramic materials starting from the same preceramic precursor, changing the flowing gas used during the ceramic conversion. Polysiloxanes have been identified as optimal preceramic materials for the production of different ceramics due to the high cross-linking rate, the wide commercials available and the suitable chemical composition [14].

1.4.   Pattern and chemical composition

PDCs are complex systems that suffer deep microstructural changes during the ceramic conversion at high temperatures. These micro domains created during the heat treatment at around 800-1000°C are also involved in the

resistance to crystallization and thermal degradation depending on the structure expansion in the resultant amorphous ceramic [15]. The formation of a nano/micro random pattern is intrinsic during the PDCs process and is mainly caused by the combustion of volatile species. In many applications, a random or specific micrometric pattern is desirable in order to expand the field of application of the synthesized materials. The main improvement carried by the microstructure, e.g. micro pores, is to highly increase the surface area. This parameter is fundamental for specific applications (discussed in following paragraphs) in which the porosity plays an important role especially in applications where is needed a high temperature, wear and corrosion resistance. Some examples are given by the filtration of molten metals and corrosive exhaust gasses, thermal insulation, catalytic reaction supports, SERS substrates and implant coatings [16]. The micrometric porosity gives to the material properties such as low thermal conductivity and mass, permeability, low density, high specific strength, low dielectric constant, modification of the refractive index and high exposed surface area. Each one of the mentioned features can be tailored controlling chemical composition and microstructure of the ceramic material [16]. Porosity changes are significant and can be changed using several shaping techniques resulting in different   pores diameter, morphology, position (open/surface/closed porosity), distribution and depth. The chemical composition has influence on electrical, magnetic, optical, chemical and biological properties. The electric conductivity of PDCs depends on different parameters including polymeric precursor, composition, pyrolysis atmosphere and temperature. In general, for SiOC, it has been demonstrated that the pyrolysis temperature largely influence the final conductivity resulting in insulator SiOC for materials converted at T < 400°C and conductor SiOC for ceramics treated at T > 1400°C. This phenomenon is explainable with the free graphitic-like carbon that is highly present in carbon-containing ceramics treated at high temperatures [2]. The inclusion of iron groups as fillers or functionalized in the final ceramic (SiOC, SiON and SiCN) leads to the formation of magnetic ceramics amplified by the presence of the SiOC matrix [17]. The presence of

6

carbon sp^2 groups, which forms an absorbing graphene layer and makes the carbon-containing ceramics black, in fact another name to indicates SiOC is "Black Glass". This characteristic hind the use of carbon-containing silicon-based ceramics as optical devices, but the intense luminescence at 500 nm given by the presence of sp^2 carbon clusters leads to a potential application as optoelectronic device. Transparent and porous SiO_2 and grey $SiON/Si_3N_4$ are widely studied nowadays as optoelectronic devices applicable in solar cells systems [18,19]. The oxidation resistance and chemical durability showed by different types of silicon-based ceramics depend on the formation, during the pyrolysis process at high temperatures, of a dense and homogeneous oxyde layer without cracks with a continuous oxide/ceramic interphase. This oxydate layer is chemically inert providing a "shell" to the ceramic material against extremely acid or basic environment, corrosion and solubilization [20–22]. The mechanical properties of PDCs strictly depends on the final shape given to the material. Different behavior have been observed shaping the ceramic in fibers, bulk or coatings. Fibers present a really high elastic modulus, with values of ~300 Gpa when to the silicon-based ceramic additives such as Ti-, Al- or Zr- are added [2]. Porous bulk PDCs present an elastic modulus range between 80 and 155 Gpa depending on the synthesis process and used precursor, with a density range of 1.85 and 2.35 g/cm^3 [23]. In the same way, also the hardness is really high depending on the pyrolysis temperature and the amount of carbon coordinated in the silicon network, in a direct relationship [2]. Porous coatings are generally used in solar cells and biomedical application to cover and protect a metal surface and also to enhance the interaction with the surrounding environment, keeping the mechanical properties of the metal below. These thin layer present porosity between 9% to 91% with flexural strength of 1–205 MPa, compressive strength of 1–600 MPa, fracture toughness of 0.3–4.3 MPa m$^{1/2}$ and thermal conductivity of 2–82 W/(m·K) [24]. One of the most important property concerning ceramic coating is the strength of the bond with the metal below in order to avoid cracks formation, delamination and debris release. In the case of Titanium, which is the most used metal for bone implant

applications, silicon-based ceramics treated at temperatures higher than 400°C, can induce the formation of an ionic bond between Ti and Si (-Ti-O-Si-) increasing the stability of the system [25].
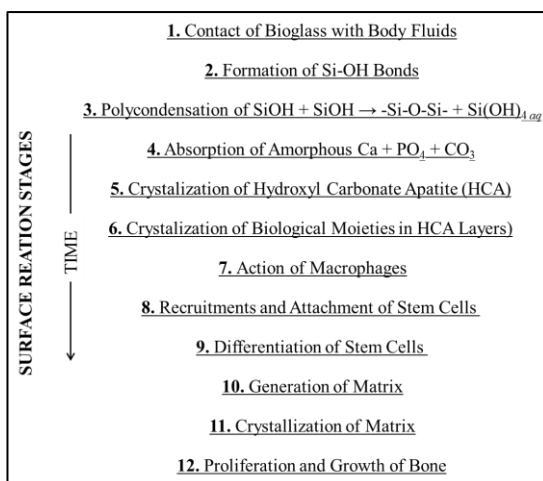
1.5. Applications

Depending on final chemical composition, microstructure and bulk shape, PDCs can be used in a wide filed of applications. Due to their specific thermal, electrical, chemical, mechanical and biological properties these material can be used in a wide range of applications. Silicon-based ceramics, including silicon dioxide (SiO_2), silicon oxycarbide (SiOC) and silicon oxynitride (SiON), are used or can be potentially used in electronical, optical, industrial and biomedical fields. It is of particular interest the application of SiO_2, SiOC and SiON porous ceramic coatings in electrical, optical and biological field [26]. Regarding SiO_2, recent studies demonstrated its high capacity, respect to graphite, in lithium battery when used as silicon mesoporous anode material [27]. Other studies revealed the good optical porous SiO_2 properties in terms of light reflection, transmission and luminescence. Monitoring the changes in these parameters when the material is in contact with a specific molecule, a porous silicon oxide sensor can be produced with a high sensibility for humidity, organic vapor, CO_x, NO_x, NH_3, O_2, H_2, HCl, SO_2, H_2S and PH_3 detection [28,29]. The same optical properties leaded to the application of porous SiO_2 coatings as anti-reflective materials in solar cells [30]. The biological classification of SiO_2 material is "inert" meaning that when is in contact with the body, no specific positive reaction are induced. For this reason, porous silicon dioxide has been proposed as middle-ear implant coating where no close contact with the physiological environment is necessary. This material was chosen for two main reasons: first of all the chemical resistance against the action of body fluids and second the easy functionalization of silanol groups in order to bind and expose molecules such as growth factors or polypeptides. The control of the surface porosity leads also to control the release kinetics of

anti-inflammatory or antibiotics uploaded to control the immunological response after implantation and to prevent possible infections [31]. Porous SiOC was also proposed in the biomedical field as porous coating for vascular prosthesis due to the interaction with blood comparable with the pyrolytic carbon but with higher mechanical and biological properties [32]. As explained before, SiOC "black glasses" possess high mechanical properties and chemical, thermal and oxidation resistance due to the high carbon content, which is both coordinated with silicon atoms or in C-C clusters increasing in this way the material properties [33]. For these reasons porous SiOC ceramics are mainly applied as coating representing a clear, transparent, protective permanent layer against weathering, corrosion and oxidation [2]. In past years, patterned SiON has been widely used for its optical properties but recently it has been proposed for biomedical applications due to the high biological properties, in particular osteoinductive effects, proven both *in vitro* and *in vivo* [25,34,35]. SiON ceramics are based on a silica network in which nitrogen is coordinated differently in a tetrahedral and trigonal disposition. The addition of nitrogen inside the network improves biological potential, mechanical-chemical resistance and improved thermal expansion coefficient of the resultant ceramic [36]. The osteoinductive mechanism is comparable with the one of Bioglasses where the ions released from the surface can induce rapid bone formation and bond on the coating surface. To synthesize patterned SiON, plasma vapor deposition is the most used technique allowing to deposit a thin layer (~200nm) on titanium surface. The patterning is usually performed on the titanium below in order to achieve a uniform vapor deposition on an already patterned surface [25]. The process is really efficient but presents some disadvantage such as the expensiveness, the high controlled atmosphere for the deposition, the titanium patterning and the controllability of the SiON deposited. Despite some drawback, Bioglasses and SiON are the most promising materials in bone healing applications due to the proven osteoinductive properties. The bioactivity of Bioglasses and SiON glasses are principally due to the release of some bioactive ions from the coating

surface when in contact with body fluids. The release mechanism was proposed by Hench *et al* and involves 12 steps starting with the immersion in body fluids and finishing with bone deposition, as reported in Table 1. The mechanism of bioactivation was deeply studied finding that the key role in the process is performed by the ions released from Bioglass, in particular the Si^{4+} (Table 1). In the human body, silicon is a trace element with a concentration in ppm. Its presence varies in body tissues, for example a concentration of 0.6 ppm is detected in blood serum, 10 ppm in liver and kidney, 40 ppm in muscle tissue, 100 ppm in bones and 600 ppm in cartilage. The principal physiological role of silicon is to working as biological bonding agent able to preserve architecture and elasticity of connective tissues [37]. Recent studies verified that silicon is fundamental for physiological bone growth and development, in fact is associated with the synthesis of collagen fibers and consecutive mineralization during the formation and development of cartilage and bone structures [38].

Table 1 Reactions involved in the bone formation process induced by Bioglasses. Adapted from [39]

SURFACE REATION STAGES — TIME

1. Contact of Bioglass with Body Fluids

2. Formation of Si-OH Bonds

3. Polycondensation of SiOH + SiOH → -Si-O-Si- + $Si(OH)_{4\,aq}$

4. Absorption of Amorphous Ca + PO_4 + CO_3

5. Crystalization of Hydroxyl Carbonate Apatite (HCA)

6. Crystalization of Biological Moieties in HCA Layers)

7. Action of Macrophages

8. Recruitments and Attachment of Stem Cells

9. Differentiation of Stem Cells

10. Generation of Matrix

11. Crystallization of Matrix

12. Proliferation and Growth of Bone

Many studies, both *in vivo* and *in vitro* demonstrated the effects of different silicon ions concentration on many osteoblasts and osteoprogenitors cell

processes. The principal role is to promote adhesion, proliferation, activation, secretion of collagen, viability and differentiation of osteoblasts and osteoprecursors such as hMSCs [40–42]. It has been observed in osteoblasts also the formation of vacuoles inside cytoplasmic vesicles with high silicon content when cells are exposed to a medium enriched with silicon ions. The role of vacuoles is still not well understood but it has been observed that cells, which present these structures, are able to secrete more ECM than cells without [43]. Form the point of view of gene expression; both osteoblasts and stem cells have been evaluated under the influence of silicon ions showing an up-regulation of fundamental genes for bone matrix formation, such as collagen type 1, alkaline phosphatase, osteocalcin, osterix, bone morphogenic protein 2 and lysyl oxidase [41–43]. A recent study also demonstrated that silicon ions are also involved in the up-regulation of super oxide dismutase type 1 which is the principal enzyme to prevent oxidative damages from radical oxygen species produced during the bone fractures [35]. The result of all these processes, when the material is applied *in vivo*, is an improved and faster bone formation on implant surface with an HCA layer closely bonded to the coating and implant fixation in the long-period [35]. Another important behavior for the silica based bioactive glasses is the formation of ionic bonds whit titanium implants (stoichiometric SiO_2-TiO_2), when thermally treated, preventing the delamination risk [25]. Regarding the biological adhesion of bone cells on SiON ceramics, also the surface pattern plays an important role. The surface pattern of a material can be defined as the combination of structures present in the nanometric (nanometers range), micrometric (micrometers) and macrometric (millimeters) range. Each one of these structure is able to direct a different cell-material or cell-cell interaction.
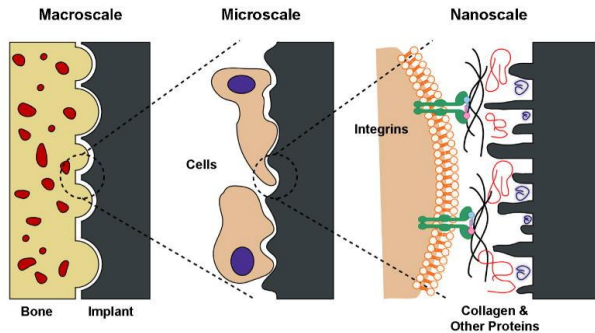
Figure 1 Bone-Implant surface interactions at macro-, micro- and nano-scale. Adapted from [44]

The first phenomenon that happens when an external material is in contact with body fluids is the protein absorption from the physiological environment. The absorbed protein layer is the main actuator of cells adhesion protein binding, in particular of integrin. The *nanometric* structure modulate quantity and types of protein absorbed directing in this way the synthesis, recruitments, grouping and bonding of different types of integrins. Integrins have dimensions in the nanometer scale (8-12 nm) and they can form aggregates called focal adhesions in the micrometric scale (1-5 µm). The substrate nanometric structure can induce the formation or the degradation of a specific type of integrins having as result the modification of cells adhesion, spreading and morphology [45]. Moreover integrins are connected to the nucleus directly or indirectly through signal transduction, in this way a specific adhesion protein can influence also cells metabolism, proliferation rate and the activity of specific enzymes [46]. Two hypotheses tried to explain the adhesion protein-nucleus communication through a mechanic transduction model: percolation and tensegrity. Forgacs *et al* formulated the percolation model in which focal adhesions are connected to the intramembrane actin filaments directly connected with the lamins in the nucleus, interconnecting in this way the plasma membrane with the nucleus [47]. Lamins are a class of structural proteins located on the nucleus and are involved in the genes transcription process. For their location and functions

12

are involved also in the second theory called tensegrity. Tensegrity (or tensional integrity) model was proposed by Ingber *et al* and involves a continuous balance between tensile elements, such as actin and intermediate filaments, and compressive elements, represented by microtubules and lamins. When the balance is moved towards one of the two parts, a specific nuclear event is induced [48].

Micrometric pattern controls cells or colony shape, adhesion, spreading, alignment, migration, aggregation and position in a phenomenon called contact guidance [49]. In this process cells recognize a specific 2D/3D pattern, such as pits, grooves, pillars, spikes and pores, which guide cells migration and, in combination with the nanostructure, the adhesion and cells spread. Through cell-cell adhesions, the cellular layer spread all over the surface assuming a specific shape that influence in a significant way their fate in terms of ECM produced and, in case of stem cells, also differentiation [50]. Unfortunately, there is not a specific value for the micrometric range, for example concerning the bone formation, different porous structures with the pores size ranging from 20 μm to 1000 μm have been proposed with controversial results present in literature [51–55]. A combination between micro topography, nano topography and nature of the material for each case of study is necessary for the biological evaluation.

The *macrometric* porosity in the millimeters range is used on the implant surface to reach the contact guidance inside the implant. This is an important factor for three main reasons: the mechanical interlocking established through the bone ingrowth that increase the fixation and the stability of the implant [56], the prevention of the epithelial down growth avoiding the fibrous capsule formation [57] and the formation of neo vascular systems into the implant surface for the new tissue maintenance [58]. For the reasons explained before, a suitable surface pattern combined with the SiON chemical composition should be present in order to maximize the positive effects of the material with the bone tissue. Nowadays, a specific pattern dimension

and structure ideal for bone cells adhesion and proliferation is still under studies. Many combinations have been tested on other cells phenotypes, but the only parameter known regards the positive effects of nanoroughness on osteoblasts and Mesenchymal Stem Cells (MSCs) [59,60].

2. *Implant coatings*

2.1. **Use of implant coatings**

Titanium and its alloys are the materials of choice for implant applications due to the high corrosion resistance, comparable elastic modulus with the cortical bone, good compressive strength and fracture toughness [61]. Despite many benefits, the percentage of implant loosening is still high nowadays and the procedure for implant substitution is really risky with the percentage of successful really lower for the second implantation. The main reason for titanium implant failure is the interaction of the metal with the bone tissue. As explained before, titanium is classified as potential "inert" material, which means that is not able to induce a direct bond with the surrounding bone [62–64]. As consequence, in load-bearing applications, the first event is the formation of a fibrotic capsule that induces the micro-motion of the implant in its site, leading to the loss and release of debris and ions [65–67]. The accumulation of debris in the fixation site leads to the acute inflammatory response, in the first period, and to a chronic inflammatory state inducing the fibrous capsule thickening and implant loosening [68]. At the same time also metal ions can be released after the titanium oxide layer damage induced by the micro-motion. Metal ions, such as titanium, aluminum and vanadium, are normally present in the body fluids but, in patients with a titanium alloy implants, the levels of these ions increase drastically [68]. The effects of these ions have been widely characterized, determining the harmful effects when they are in high concentration. Aluminum is associated with bone growth inhibition, Alzheimer's disease, hypersensitivity, carcinogenesis and kidney damages when systematically present in high concentrations [69–71]. Vanadium presents a comparable harmfulness, having been associated with cardiac and

renal dysfunction, hypertension, incomplete reproductive development, psychosis and carcinogenesis [68,72,73]. On the other hand, the role of titanium ions in toxicity is still under study but it is well known that the ions released from the implant surface react immediately with water and anion species forming titanium oxides and salts which are able to easily react with amino acids compromising their functions [74]. To overcome all these problems and to guide a correct biological response, researchers proposed to use implant coatings to achieve rapid and strong bone-material bond. Using coatings, it is possible to modify the surface chemistry, topography, roughness and energy of the material in contact with the bone tissue preserving the mechanical properties of the coated metal. On the base of the host response to the coatings, they can be divided into biotolerant, bioresorbable and bioactive. Biotolerant materials cannot be used due to the formation of a thin fibrous layer which leads to the implant rejection. Bioresorbable materials, after the resorption and substitution with bone tissue, expose the new formed bone with the metal implants bringing back all the problems already explained. For these reasons the best choices are the bioactive materials, which are able to induce strong implant integration through direct material-bone bond [75]. The most promising materials that belong to this category are: titanium nitride, biological coatings, hydroxyapatite and bioactive glasses and ceramics.

2.2. Titanium nitride

Titanium nitride is a promising coating for titanium implants obtained through physical vapor deposition techniques on the implant surface. The addiction of nitride compounds shows an improved biological activity compared to the titanium and its alloys. The main advantages for these coatings are two: the strong implant-coating bond and the improved biological activity [76]. Using the vapor deposition technique, titanium nitride and the thin oxide layer on titanium implants are strictly bonded because the substrate is directly involved in the formation of the coating layer. Titanium

oxide induce the formation of an intermixed layer which indicates the strong adhesion between substrate and nitride film [77]. The improved biological activity is probably due to the exposed nitride groups which enhance the blood compatibility, specific proteins absorption and platelet retention resulting in a rapid and profitable interaction with the bone [78]. As result of the combination of these two phenomena, a coating with good mechanical and biological characteristics has been synthesized. The strong bond allows to prevent coating delamination, debris release and increase wear resistance. *In vivo* studies demonstrated a good osteointegration of the implant with the coating compared to the commercial pure titanium and its alloy showing a good bone ingrowth and surface bond, no fibrous capsule formation and expression of enzymes and markers related to the bone-cells differentiation [79]. Despite many benefits, the synthesis techniques of this material present some drawbacks. The main disadvantages are in the thickness and surface pattern control of the coating during the deposition. Using the vapor deposition a non-uniform layer, with a thickness in the nanometers range, is deposited on the implant surface in a really complicated temperature-dependent process [80].

2.3. Biological coatings

The term biological coating refers to the functionalization of a material with biological molecules that induces bone formation acting on differentiated and undifferentiated cells to achieve osteointegration [81]. In order to promote bone formation, molecules such as growth factors or recognition sequences, are integrated on a coating with a biomimetic structure. Usually these molecules are integrated on a polymeric surface synthesized with a specific bone-like structure. The most promising are the amino acidic sequences, arginine, glycine and asparagine (RGD) and the growth factors called bone morphogenetic protein (BMP).

RGD. A sequence of three amino acids, arginine, glycine and asparagine, can be recognize by bone cells inducing adhesion, proliferation and

differentiation starting the bone healing process in their vicinity [82]. The main advantages of use a short peptides sequence instead of an entire protein are the dimensions and the easier synthesis process and functionalization method. RGD sequences are more stable than the entire proteins and the same surface area can be functionalized with a denser amino acidic layer [83]. Recent studies demonstrated the efficacy in osteoblastic cells adhesion, proliferation and differentiation induction [84]. Despite many benefits *in vitro*, *in vivo* studies are not still complete showing lower performances compared with bioceramics and bioglasses coatings probably due to the interactions with the body fluids [83].

BMP. Bone morphogenetic proteins are a family of growth factors already used in clinical applications. The most used is BMP-2 which plays a fundamental role in bone remodeling processes enhancing bone healing and increasing bone volume and density when used with low dosage [85]. On the other hand, a high dosage can induce bone resorption acting directly on osteoclasts differentiation and proliferation [81]. The key issue, to use this protein functionalized on a coating, is to control the release kinetics. There are many techniques that can incorporate BMP into the coating materials, but all of them result in a burst release where a continuous and gradual low release is needed [86]. Researchers are moving to a controlled drug-delivery system to induce a specific release kinetic once implanted, but the high expensiveness of BMP makes really difficult the usage and the experimental tests.

Both the described materials present some disadvantages that make the application really complicate. The main problems related with biological molecules refer to their instability in a multicomponent environment such as the human body. Factors such as pH changes, bacterial activity, inflammatory response, not specific cells interactions, inactivation of the compound, changes in temperature, specific patients responses, release rate

and concentration effects make these biomolecules really hard to use in clinical field and also to preserve their functionality in the human body [81].

2.4. Hydroxyapatite

The mineral constituent of bone tissue is called biological apatite. This material is an impure form of the mineral Hydroxyapatite (HA, $Ca_{10}(PO_4)_6(OH)_2$) in which some phosphonate ions, $(PO_4)^{3-}$, are replaced with carbonate ions, $(CO_3)^{2-}$, and the surface of the crystals is incorporated with other ions such as Na^+, K^+, Mg^{2+}, F^- and Cl^- [87]. Hydroxyapatite (HA) coatings are part of the calcium phosphate ceramic family. These materials are widely use because are found, in different forms, in the bone tissue providing an improved osteoconductive effect both *in vitro* and *in vivo* [88,89]. *In vitro* studies on osteoblasts cultures, grown on HA layer, demonstrated the expression of many osteogenic markers, such as alkaline phosphatase activity, parathyroid hormone secretion, osteocalcin expression and collagen type I deposition, compared to the commercial pure titanium and its alloys [90]. The effects on osteoblasts progenitors has also been evaluated showing an enhanced expression of osteogenic genes [91]. *In vivo* studies show a no fibrous capsule formation, no inflammatory cells infiltration in implant-bone space and an increased resistance to shear forces created during the implant insertion [92,93]. Moreover, an improved osteointegration and osteoconduction can be achieved synthesizing the coating with a specific topography in terms of micrometric porosity and nanometric roughness [94]. The osteoinductive effect given by the presence of HA is probably due to the particular combination in surface energy and topography. It has been demonstrated that HA surfaces *in vivo* can absorb from the body fluids growth factors, which are fundamental for osteoblasts activation and osteoprogenitors differentiation. At the same time, the bone-like nanostructure and chemical composition, are ideal for bone cells adhesion and activation through the expression of specifics integrins [91]. Also the micrometric structure plays an important role promoting cells penetration and bone ingrowth when

synthesized in specific ranges [89]. For these reasons, HA coatings are the most promising materials for bone integration. The efficiency is strictly dependent on the final crystalline structure and on the metal-ceramic bond strength, which are both parameters resultant from the synthesis method. The most used technique to coat metal implants with an HA layer is the plasma spraying [81]. Over the problems of the uniform layer production with a specific microstructure, this technique presents also other issues. For example the elevated temperatures reached during the process can modify the HA crystalline structure making the coating prone to fractures and adhesion failure [95]. Also the long-term performances are still under studies due to the tendency of HA to dissolve in physiological environment creating amorphous $Ca_3(PO_4)_2$ which is responsible for coating delamination and detachment [96].

2.5. Bioactive glasses and ceramics

With the terms bioactive ceramics and bioactive glasses we refer to glass or ceramic materials used for the repair, replacement or reconstruction of a damaged part of the body. In the past years, polycrystalline (e.g. alumina), bioactive glasses, bioactive glass-ceramic (e.g. apatite/wollastonite) or bioactive composite (e.g. polyethylene-hydroxyapatite) have been used for the fixation of musculo-skeletal system such as repair of bones, joints or teeth [97].

Table 2 Classification of bioactive ceramics and glasses on the base of tissue attachment and host response. Adapted from [39]

Type of attachment	Type of bioceramic
Dense, nonporous, almost inert ceramics attach by bone growth into surface irregularities by cementing the device into the tissue, or by press-fitting into a defect (morphological fixation).	Al_2O_3 ZrO_2
For porous implants, bone ingrowth occurs, which mechanically attaches the bone to the material (biological fixation).	Porous hydroxyapatite Hydroxyapatite-coated porous metals
Surface-reactive ceramics, glasses, and glass-ceramics attach directly by chemical bonding with the bone (bioactive fixation).	Bioactive glasses Bioactve glass-ceramics Dense hydroxyapatite
Resorbable ceramics and glasses in bulk or powder form designed to be slowly replaced by bone.	Calcium sulfate (plaster of Paris) Tricalcium phosphate Calcium phosphate salts Bioactive glasses

These materials can be divided in four categories on the base of the final fixation occurred after implantation: morphological, biological, bioactive and resorbable fixation (Table 1). Morphological fixation is achieved when a dense ceramic coating is mechanically fixed, using an adhesive agent, in the bone tissue. Bone adhesion ensures a more stable implantation compared to a cementless prosthesis, resulting in increased mechanical properties during the long-period. This is the case of "inert" ceramics such as alumina or zirconia. Biological fixation refers to the implantation of porous (100-150 μm) ceramics mechanically placed into the bone tissue. The bone ingrowth into the interconnected porosity ensures a deeper fixation in the long period if compared to a flat coating, like in the case of hydroxyapatite. As explained before, resorbable materials are a good choice for non-union bone fractures where a scaffold is needed to drive the bone replacement. Used as coating for metal implants, these ceramics can drive the bone replacement regulating the inflammatory response, but when is completely resorbed, the below metal surface is completely exposed to the body. The ideal solution for implant integration is to achieve the bioactive fixation in which the material undergoes to a time-dependent surface modifications resulting in a formation and bond of a HCA layer with the coating [39]. This phenomenon is peculiarity of a glasses family discovered by Hench and co-workers in 1960s called Bioglass. Bioglasses are a silica based glasses containing in different proportions SiO_2, Na_2O, CaO and P_2O_5 [39]. Bioglass 45S5 is the most studied and used for bone repair, is composed of (%wt): 45% SiO_2 - 24% 5CaO - 24% $5Na_2O$ - 6% P_2O_5) and shows osteoconductive and osteoinductive properties [98]. With the passing years, other bioactive glasses have been synthesized and tested to overcome some disadvantages. For example, to match the titanium thermal expansion, these materials have been added with MgO but, further studies, demonstrated that Mg^{2+} released from the surface down-regulates important osteogenic markers resulting in slower bone formation and possible implant loosening [42]. Moreover, synthesis techniques, for the production of a patterned ceramic, are very expensive, time consuming and can give a non-uniform implant coating, resulting in

implant failure [99]. To overcome these problems, new silicon based materials have been studied. In particular, amorphous Silicon Oxynitride (SiON) glasses represent an alternative material, which exhibits osteoinductive properties both *in vitro* and *in vivo* [25,35]. SiON ceramics are based on a silica network in which nitrogen is coordinated differently in a tetrahedral and trigonal disposition. The addition of nitrogen inside the network improves biological potential, mechanical-chemical resistance and improved thermal expansion coefficient of the resultant ceramic [36]. The osteoinductive mechanism is comparable with the one of Bioglasses where the ions released from the surface can induce rapid bone formation and bond on the coating surface. To synthesize patterned SiON, plasma vapor deposition is the most used technique allowing to deposit a thin layer (~200nm) on titanium surface. The patterning is usually performed on the titanium below in order to achieve a uniform vapor deposition on an already patterned surface [25]. The process is really efficient but presents some disadvantage such as the expensiveness, the high controlled atmosphere for the deposition, the titanium patterning and the controllability of the SiON deposited. Despite some drawback, Bioglasses and SiON are the most promising materials in bone healing applications due to the proven osteoinductive properties. The bioactivity of Bioglasses and SiON glasses are principally due to the release of some bioactive ions from the coating surface when in contact with body fluids. The release mechanism was proposed by Hench *et al* and involves 12 steps starting with the immersion in body fluids and finishing with bone deposition, as reported in table 2. The mechanism of bioactivation was deeply studied finding that the key role in the process is performed by the ions released from Bioglass, in particular the Si^{4+} (Table 2). In the human body, silicon is a trace element with a concentration in ppm. Its presence varies in body tissues, for example a concentration of 0.6 ppm is detected in blood serum, 10 ppm in liver and kidney, 40 ppm in muscle tissue, 100 ppm in bones and 600 ppm in cartilage. The principal physiological role of silicon is to working as biological bonding agent able to preserve architecture and elasticity of connective tissues [37]. Recent studies verified that silicon is

fundamental for physiological bone growth and development, in fact is associated with the synthesis of collagen fibers and consecutive mineralization during the formation and development of cartilage and bone structures [38].

Table 3 Reactions involved in the bone formation process induced by Bioglasses. Adapted from [39]

SURFACE REATION STAGES	TIME	
		1. Contact of Bioglass with Body Fluids
		2. Formation of Si-OH Bonds
		3. Polycondensation of SiOH + SiOH → -Si-O-Si- + Si(OH)$_{4\ aq}$
		4. Absorption of Amorphous Ca + PO$_4$ + CO$_3$
		5. Crystalization of Hydroxyl Carbonate Apatite (HCA)
		6. Crystalization of Biological Moieties in HCA Layers
		7. Action of Macrophages
		8. Recruitments and Attachment of Stem Cells
		9. Differentiation of Stem Cells
		10. Generation of Matrix
		11. Crystallization of Matrix
		12. Proliferation and Growth of Bone

Many studies, both *in vivo* and *in vitro* demonstrated the effects of different silicon ions concentration on many osteoblasts and osteoprogenitors cell processes. The principal role is to promote adhesion, proliferation, activation, secretion of collagen, viability and differentiation of osteoblasts and osteoprecursors such as hMSCs [40–42]. It has been observed in osteoblasts also the formation of vacuoles inside cytoplasmic vesicles with high silicon content when cells are exposed to a medium enriched with silicon ions. The role of vacuoles is still not well understood but it has been observed that cells, which present these structures, are able to secrete more ECM than cells without [43]. Form the point of view of gene expression; both osteoblasts and stem cells have been evaluated under the influence of silicon ions showing an up-regulation of fundamental genes for bone matrix formation, such as collagen type 1, alkaline phosphatase, osteocalcin, osterix, bone morphogenic protein 2 and lysyl oxidase [41–43]. A recent study also demonstrated that silicon ions are also involved in the up-regulation of super oxide dismutase type 1 which is the principal enzyme to prevent

oxidative damages from radical oxygen species produced during the bone fractures [35]. The result of all these processes, when the material is applied *in vivo*, is an improved and faster bone formation on implant surface with an HCA layer closely bonded to the coating and implant fixation in the long-period [35]. Another important behavior for the silica based bioactive glasses is the formation of ionic bonds whit titanium implants (stoichiometric SiO_2-TiO_2), when thermally treated, preventing the delamination risk [25].

3.   Patterning techniques

3.1. Background

An interesting characteristic of PDCs is that they are in a high viscous liquid state before the heat treatment for the ceramic conversion. It means that they can be processed using different techniques in order to impress a specific pattern to the final ceramic. In this way they can be subjected to a variety of forming methods, some of them specific or easily applicable for PDCs respect to the ceramic paste. For this reason, the PDCs approach has interesting technological advantages if compared to the use of other molecular precursors. The drying time required for the process do not represent a problem for the final material, giving the possibility to modify the ceramic molten state imprinting a specific 3D pattern. The PDCs solutions are stable in time, they are generally cheap, commercially available and they do not need specialized handling procedures [2]. Nowadays there are three principal routes to obtain a ceramic surface with a specific pattern: lithographic, coating processes and self-assembly techniques.

3.2. Lithographic techniques

Lithographic methods are widely used in the semiconductor field to imprint a micro texture on electronic devices. The most used lithographic technique is called photolithography and involves multiple steps to obtain a patterned surface. The first step involves the deposition of a photo-curable coating (photo resist) on the substrate to pattern. In the second step the photo resist is

irradiated with a radiation passing through a mask with the desired pattern, so that only specific parts of the resist interact with the radiation changing its physical properties. This step includes also the removal of the photo resist in the spaces not covered by the mask. Once the resist is selectively removed, the below substrate is exposed to the action of ion-etching or ion-implanting in order to imprint a specific patter in the areas not covered by the resist. The last step involves the complete removal of the photo resist freeing the patterned structure [100]. In last years, several improvements have been applied to the lithographic techniques enhancing the efficiency, reproducibility and resolution of the process using new types of lenses, different radiation sources and new types of masks. Photolithography has been used to pattern either directly the surface of titanium implants or the coating applied. Nowadays, in the biomedical field, this technique is not used anymore because of some disadvantage involved in the process. The first one is the need for a photo resist that cannot be reused for each process, which represent a big issue especially regarding the industrial production, where a mass scale-up process is required. Regarding the use of ceramics as metal coatings, there are some limitation concerning the coating-implant adhesion in the case of patterned implant coatings, being photolithography just a subtractive technique, without further material additive capability. In this case another synthesis method must be applied to deposit the material inducing, at the same time, a strong adhesion. By combining lithography with other techniques, many different coatings can be obtained, but together with an increase in expensiveness and duration of the pattern process [101]. Despite these disadvantages, photolithography represent a powerful technique and it has been taken as model for the development of other process that can combine the deposition of a coating with the specific pattern applied on the surface.

3.3. Coating techniques

Coating techniques are processes in which a coating is synthesized directly on the material giving a specific pattern in one step. Different techniques can influence the characteristics of the final coating in terms of adhesion strength, thickness uniformity, pattern resolution and chemical modifications. The principal methods used for this application are: plasma sprayed deposition, hot isostatic pressing, thermal spray, dip coating, pulsed laser deposition, electrophoretic deposition, sol-gel and ion beam assisted deposition.

Plasma spray. This technique involves the melting of the ceramic or metal, to use as coating, through heat ionized inert gas or plasma. The molten material, in different ratios, is then sprayed on the metal surface, forming the protective layer with a porous random pattern inducing at the same time the ceramic conversion due to the high temperatures used. Advantages using this technique concern the rapid deposition and the low coast of each process. In addition, there are lower risks of thermal degradation of the used material if compared with other high temperatures used in similar techniques. The main problems with plasma spray are the low control on the surface topography and resolution formed during the process, structural changes in the coating microstructure, which leads to fractures, and the poor induced adhesion between coating and metal implant [102,103].

Hot isostatic pressing. Hot pressing is a process in which, by using a pressurized gas, the coating is pressed on the implant surface to imprint the required load at specific temperatures. To perform this process, the coating in powder or in liquid state and titanium (substrate) are pressed together using a glass or metal encapsulation chamber in which gas is introduced to reach a pressure of 100-320 MPa and temperatures up to 2000°C. The process is normally performed for ceramic coatings in large industrial equipment with a high control on temperatures, pressures and on all the process variables allowing the production of a dense, net shaped materials

with superior and consistent properties. Temperatures and pressures reached during this process are the biggest disadvantages that can be applied only in specific devices with a really high control on the process environment. Moreover, it has been demonstrated that the bond strength depends on the reached temperatures and on the thickness of the applied coatings. In general the thinner is the layer, the stronger is the bond and vice versa, resulting in a really strong bond only for layers thinner than 100 μm [104,105].

Thermal spray. The process starts from melting the ceramic precursor in powder through the use of different energetic sources, such as flame, electricity or plasma. The semi-molten heated material is then accelerated and expelled on a prepared surface by gasses or atomization jets. Thermal spray of coatings is a relative new technique, and presents still many issues to overcome. One is the difficulty to impress a specific pattern to the sprayed material or to set the energy level required to perform the process. In addition, the high sintering temperatures used can allow to crack propagation on the coating surface, poor adherence and non-uniform crystallinity [106,107].

Dip coating. In this technique the metal substrate is immersed in a liquid containing the dissolved precursor, and then extracted at constant speed. During the extraction phase, a thin liquid film is left on the metal surface. The thickness of the film is correlated with the extraction speed and can range between 0.05 and 0.5 mm. At the end of the process the organic solvent used is left to evaporate, generating the consolidation of the solute present in the solution. Normally, an additionally curing or sintering phase is necessary to consolidate the material adhesion, to generate the ceramic conversion and to induce the evaporation of all the organic solvent, and any side chemical reactions, generating a strong bond. The low cost, simple steps and high coating quality produced from this process made the dip coating really popular and efficient. In order to have a specific pattern on the coating substrate at the end of the process, the metal implant must be already patterned and for this reason dip coating approach loses appeal from a

production point of view. Researchers proposed UV cross-linkable materials to use as coating, in a simil-photolitography process, and to polymerize immediately after the extraction step, but the process is still under studies for the ceramic coating synthesis [108,109].

Pulsed laser deposition. In last decades, laser has been used in biomedical applications to create microstructures, to enhance the biofunctionality and, recently, also for materials deposition. Pulsed laser deposition involves the vaporization of the coating material through laser energy. The vapor is then ejected and condensed on the metal surface. Repetition of the deposition cycles allows the formation of a patterned coating with no changes in material stoichiometry or crystallinity. The main limitations of this technique are the expensiveness of the device, the low controllability, the ranges of pattern obtainable and the material splashing due to the slow-moving particulates [110].

Electrophoretic deposition. Electrophoretic depositions are a family of techniques in which particles in a suspension are bind onto an electrode under the influence of an electric field. These techniques present many advantages, in particular regarding the easy and fast process, the simple used devices and the obtainable ranges between 1 mm and about 100 μm. Taking into consideration the advantages mentioned above, electrophoretic deposition has been proposed also for implant coating deposition, but the applicability is still hard to perform due to the difficulty in control the surface pattern during the process and to the low adhesion of the material on the implant surface [111,112].

Sol-Gel deposition. This process is the simplest, among the other previously mentioned, to produce multicomponent oxide coatings. The method involves the production of a solid material starting from a solution in which the precursor is dissolved in monomeric, oligomeric or polymeric forms. The transition involves four steps: 1) formation of a solution of purified precursor in an organic solvent miscible with water (sol); 2) convert the sol

27

to gel through polycondensation; 3) shaping the gel to a specific patterned form and then 4) fixing the shaped gel through sintering at 500 °C [113]. The process itself possess numerous advantages such as optimal adhesion between coating and substrate, formation of a thick layer, possibility to precisely shape the gel into many forms, production of high purity coatings and the effectiveness, simplicity and inexpensiveness of the process [114]. On the other hand, some disadvantages could arise, such as the low wear resistance, the high permeability, the inclusion of organic molecules during the sintering and the difficulty to control the porosity during the process [114].

Ion beam assisted deposition. This technique is a combination between vapor deposition and ion beam bombardment, performed in vacuum. The main advantage of this technique is the resulting adhesive strength of the final coating on the metal implant due to the bombardment with an ion beam with a specific energy that cause the interaction between the coating and metal substrate ions, forming an intermixed zone. In the process, many factors and parameters need to be controlled and evaluated to induce the right mechanical, structural and chemical properties. These parameters, among which evaporation or sputtering rate, ion beam energy, density and species, are generally difficult to control and combine properly without the adoption of advanced devices, the only way to ensure the reproducibility of the synthesized ceramic [115,116].

3.4. Self-Assembly Techniques

Self-assembly (SA) is a process in which molecules, present in a solution, form an organized and patterned structure exploiting local and specific interactions without external interventions. This process allows the formation of structures with a specific 2D or 3D porous pattern using really fast and inexpensive techniques [117]. The first property of SA materials is the process spontaneity, which acts in a local level driving the interphases forces for the final material formation. The three distinctive characteristics of the SA process are the order, the interactions and the building blocks. The order

regards the system entropy decrease passing from the initial non-assembled, through the formation of building blocks and, in the end, to the final shaped material. The types of molecular interactions involved in the SA method are in general the forces that drive the biological interactions, such as hydrogen bonds, thermocapillary forces and Van der Waals interactions. In the end, after the molecular levels, the material building blocks are self-organized forming a fast and controlled architecture [118]. Many methods have been developed taking advantages of the SA phenomena and the most used nowadays are colloidal crystal templating, emulsion droplet templating, phase separation and the Breath Figure (BF) method.

Colloidal crystal templating. This method involves the formation of high-packed sacrificial 3D structures of nanometric or micrometric beads through centrifugation, deposition, sedimentation or filtration of a suspension. The materials commonly used as "fillers" are polystyrene, latex and silica due to the high controllability in dimension and for the easy removal. After the template formation, voids around the beads are filled with a solution that after polymerization, sol-gel process or precipitation solidifies generating the porous structure. The final step involves the complete removal of the beads aggregates by physical or chemical dissolution, leaving the final 3D structure which is the negative of the sacrificial template. The principal advantages of these techniques are the uniformity and monodispersion of the final pores array though, usually, defects and randomly oriented domains are present. The removal of the sacrificial template can damage the porous structure and it is not possible to recover the template material after each process. Despite some disadvantages, this method allows to synthesize high regular porous structures with a good interconnectivity and high controllable pores diameter depending on the beads size [119].

Emulsion droplet templating. In the emulsion droplet templating, the sacrificial structure is represented by a high-packed 3D aggregate of emulsion droplet. The working solution is composed of the liquid form of

the material precursor and by droplets or beads created by emulsion. A centrifuge step aggregates the droplets in a high-packed state and then the material solidification is induced usually by pH modifications. The template is usually removed through washing in organic solvent. This technique is the least used, between the SA techniques, due to the high irregularities and defects in the final product, the low reproducibility and the difficulty in control emulsion pores distribution [120].

Phase separation method. Controlled phase separation process involves the separation between covalent bonded block copolymers. Each copolymer has a specific side-chain which can confer to the same material different properties, for example, when the parts are immiscible, solidification leads to phase separation. The process is accompanied with the formation of a porous pattern, generally, with a low degree of regularity. This method is widely used for the formation of polymeric membranes used as gas filters or biosensors, but there are few usable precursors for the process which give a nanometric patter with lamellar, cylindrical or spherical domains [121].

Breath Figure method. Concerning the SA processes, the most promising technique is called Breath Figure (BF) method. This technique uses as template, for the pattern formation, a regular array of condensed water drops on a solution surface. Using a solution composed of an organic solvent with a low boiling temperature casted in a humid environment, the evaporative cooling leads to the condensation of water droplets on the solution surface. During the process, the material solidification is induced around the droplets which penetrate and float on the solution surface acting as removable template. After the solidification and evaporation of water and solvent, a solid surface porous film is left on the used substrate. Compared to the other methods, BF technique is faster and cheaper and can be made using homemade devices using a wide range of precursors, from polymers to organic and inorganic materials with a high controllability on the final surface pattern [122,123].

Besides the techniques based on SA process, other methods can be used to obtain porous structures such as freeze drying, salt-leaching, fiber bonding and electrospinning. The results for these processes are really hard to control and reproduce, with a non-uniform pores dimension and a difficult coating of 3D materials.

4. Breath Figure method

4.1. Introduction

The BF mechanism was first investigated by John Atken in 1885 and defined by Lord Rayleigh in 1911 who characterized the morphology of the droplets array during the process [124]. After the discover, BF process was consider a natural phenomenon without practical applications until 1994 when Françoise *et al* reported the preparation of a typical micrometric honeycomb array using a solution of polystyrene-b-polyparaphenylene in carbon disulfide [125]. The relationship between the work of Françoise and Lord Rayleigh was recognized, discovering a new possibility to obtain a high-packed pores array on material surfaces. In the last two decades, BF method has been used to imprint a surface porous pattern on a wide range of materials such as: linear, branch, star and biodegradable polymers, microgels, nanoparticles, graphene, carbon nanotubes and small organic molecules [124]. Moreover, depth studies, allow to the possibility to modulate the pattern geometry, in terms of pores diameter, shape, depth and density, simply modifying the variables involved in the process. Compared with the techniques described above, BF presents many advantages: 1) low cost process with home-made devices; 2) time-saving one-step procedure allowing to pattern many surfaces in minutes; 3) easy procedure and finely controllable variables; 4) highly reproducible results; 5) a wide range of surface pattern can be obtained expanding fields of application. For this last reason, BF have been proposed for a wide range of applications such as templates, Surface Enhanced Raman Spectroscopy (SERS) substrates, separation membranes, picobeaker, molecular sieves, optical and

optoelectronic devices, chemical power sources, micropatterning for biological molecules, sensors and substrates for cell growth [126].

The BF process starts with the dissolution of the chosen precursor in an organic solvent with a low boiling point. A specific amount of the starting solution is than casted under the influence of a humid environment. The evaporative cooling of the solvent generates a temperature gradient inducing the condensation of water droplets and subsequent organization in a high-packed array. In this phase is fundamental the choice of the right organic solvent considering properties such as volatility, latent evaporation heath, water miscibility, gravitational effects and surface tension. The solvent golden standards are represented by chloroform, ethyl acetate, carbon disulfide, toluene and dichloromethane. After the complete water and solvent evaporation, a surface porous film is left on the substrate thanks to the imprint of the droplets array [127]. The BF process can be divided into three phases:

1)   *Initial stage.* Water drops start to condense and nucleate on the solution surface due to the temperature difference induced by evaporative cooling. In this stage, drops formed are small and the surface cover is low. Once condensed, droplets increase their diameter by acquiring humidity from the environment following equation 1.1 where D is the diameter of the drops and t is the time:

$$D \propto t^{1/3}$$

[1.1]

2)   *Intermediate stage.* In this stage the droplets coverage on the solution surface reach its maximum. The phase is characterized by a drastic decrease in system entropy in which droplets are arranged in a close-packed honeycomb array. The result is an array in which each drop is surrounded by other six and the diameter is monodisperse.

3)   *Final stage.* This is a coalescence-dominated stage in which droplets cover the entire available surface. Droplets coalescence leads to a continuous re-arrangement of the array with a consequent drastic decrease in system order. This phase follows equation 1.2:

$$D \propto t$$

[1.2]

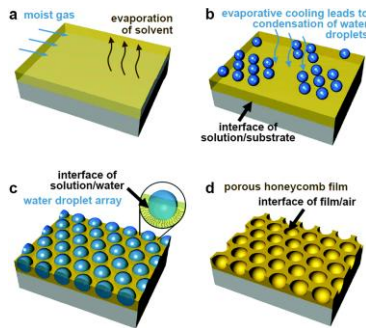A schematic representation of the BF method phases is represented in figure 3:

Figure 3 Schematic representation of the BF process. Adapted from [128]

4.2. Initial stage

In the initial stage of the BF process, nucleation and drops formation occurs randomly on the liquid surface and in a low number. These features strictly depend on the difference in temperature between liquid surface and environment and also on the substrate wettability and water miscibility with the solvent. The nucleation and growth of a water drop locally deform the system continuity creating three different interfaces as shown in figure 4:
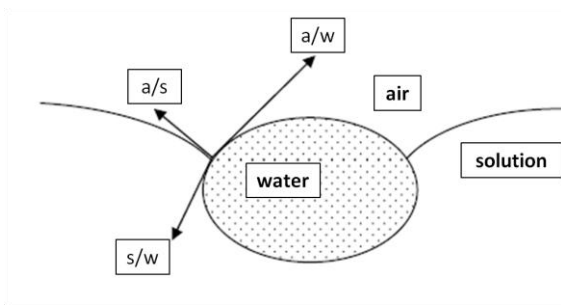
Figure 4 Droplet on the solution surface

In this case drops are in equilibrium, interrupting the continuity of the liquid. Buoyancy, and resultant solution bending, are the result of gravity and capillary forces [129]. It has been demonstrated that liquid bending plays an important role in droplets aggregation, inducing long-range elastic interactions and changes between the forces derived from the surface tension [129]. During the initial stage, droplets deposition is driven by the solution surface deformation and by the convective motion of the evaporating solution. Another important parameter to take in consideration in this stage is the nucleation rate (J) intended as the number of droplets formed on a defined surface at a specific time point (n° droplets/cm^{2}s). This value principally depends on the energy required for the nucleation ($\Delta\Omega$), temperature (T) and Boltzmann's constant (k) as described in equation 1.3:

$$J = J_0 \, \exp{-\frac{\Delta\Omega}{kT}}$$

[1.3]

By definition, the parameter $\Delta\Omega$ depends on the air/water surface tension (γ_w), on the droplet shape (f), which depends on the contact angle of water on the polymeric surface, on difference in water partial pressure in the gas phase and vapor pressure at liquid interface (ΔP) as described in equation 1.4:

$$\Delta\Omega = \frac{16\pi\gamma^2_{a/w}f}{3\,(\Delta P)^2}$$

<div align="right">[1.4]</div>

Combining equation 1.3 and 1.4, an evaluation of the principal parameters involved in the nucleation rate can be obtained:

$$J \propto exp - \left(\frac{16\pi\gamma^3_{a/w}f}{3(\Delta P)^2 kT}\right)$$

<div align="right">[1.5]</div>

Considering equation 1.5 it is clear that a decrease in contact angle value leads to a faster nucleation with consecutive higher final number of pores on the film surface [130]. Considering the same solvent in a completely covered high-packed surface, the number of pores remains constant regardless of the pores size. As a consequence, the pores diameter depends on the number of pores present on a specific area, which depends in turn on the nucleation rate. In the initial stage it is possible to assume that the final pores size is inversely proportional to the nucleation rate and, from equation 1.5, to the wettability of the polymeric solution. The nature of polymer and solvent, as well as the presence of surfactants in the solution, affects the interfacial tensions at water/solution ($\gamma_{w/s}$) and water/air ($\gamma_{w/a}$) phases . This leads to a disproportion in terms of surface energy between the top of the drop and its base inducing Marangoni convection, which forms a thin polymer layer on the drop top side decreasing the energy [131]. If the polymer, the solvent or surfactant interact with the water decreasing $\gamma_{w/a}$, the wettability decrease leads to a faster nucleation.

4.3. Involved phenomena

The temperature gradient in the BF process causes the mass transfer in liquid following a phenomenon called convective motion. Taking in consideration

a liquid layer, the temperature gradient induces a density variation causing the formation of cooler and hotter convective cells. For gravity effects, cooler and less dense cells tend to sink, while hotter and more dense cells tend to float. The floating is supported by buoyancy forces called Rayleigh convection, which is opposed by viscous drag and heat diffusion. Viscous drag is a force opposite to the flow and is dependent on the solution viscosity. The viscosity of the polymeric solution represents, in this case, the indication of the energy required to promote a mass transfer on a specific polymeric solution. Heat diffusion tends to equalize the vertical temperature gradient slowing the mass motion and depends on the liquid thermal diffusion. If the thermal diffusion value is high, the reduction of the temperature gradient is fast without fluid motion, otherwise the gradient reduction occurs preferentially through mass transports. The Rayleigh number (R) represents the ratio between buoyant forces and opposite viscous drag and heat diffusion:

$$R = \frac{ga\Delta T d^3}{vk}$$

[1.6]

where a represents the thermal expansion coefficient, ΔT is the vertical temperature gradient, d is the liquid layer thickness, g is the gravity, v is the viscosity and k represents the thermal diffusivity of the liquid. Being R a ratio between forces, if the buoyant force dominates the process, convective cells are forming (high R value), otherwise if the dissipative forces dominates the process, no mass transfer occurs (low R value) [132]. Another aspect to take into consideration in the BF process, is the surface tension modification caused by the temperature gradient. Surface tension is a function of temperature and decrease reaching the liquid-vapor critical point where the surface tension is zero. In BF process, the modification of the surface tension is induced also by the presence of surfactants inside the polymeric solution or by the formation of a concentration gradient. The

result is the fluid motion from regions with a low surface tension to regions with high values in order to reach the energy minimization decreasing the high surface tension areas. Considering the temperature gradient, fluid motion tends to move from warmer areas to cooler areas with opposite forces represented once more by viscous drag and heat diffusion. Even in this case, if the dissipative forces are higher than the gradient, fluid motion occurs (Marangoni convection). Taking in consideration the case in which surface tension is modified by temperature gradient, the process is called thermo-capillary convection [133]. To predict the evolution of a system, Marangoni number (M) has to be take into consideration:

$$M = \frac{\gamma' \Delta T d}{pvk}$$

[1.7]

Where γ' is the temperature derivative from surface tension, p is the density of the polymeric solution at a specific temperature and other values have been described above. Even in this case, as in equation 1.6, the fluid movements happen if Marangoni number exceed a specific value, which represent the best contribution of surface tension gradient respect to the dissipative forces. In this case, Marangoni convection causes the formation of convective cells in which fluid flows ascending in the center and descending on the edges of the cells. This phenomenon is linked with the convection motion described above and induces the depression of the cells center. Combining equations 1.6 and 1.7 the ratio between Marangoni and Rayleigh numbers gives information about the dominant process:

$$\frac{R}{M} = (\frac{pag}{\gamma'})d^2$$

[1.8]

During the BF process, both the convections (R and M) occur together, with cases in which one is predominant and the effect of the other is irrelevant. For example, being the ratio dependent on the film thickness, Marangoni convection will be more important in case of thin liquid layers while convective motion will be predominant in case of thick layers.

4.4. Intermediate stage

The intermediate stage occurs when the droplets coverage reaches its maximum. In this part, the non-coalescence plays an important role to have a monodisperse diameter values on the final surface, despite it has been demonstrated that coalescence can occur at every stage of the process. The perfect BF process allows the formation of hexagonal pores array (honeycomb structure) following the hard-spheres-like interactions, which minimize the system energy. The non-coalescence effect is a multi-components phenomenon, which involves all the parts of the BF system. One reason for the non-coalescence effect is the formation of a compressed polymer layer between each drop. This layer is the result of polymer precipitation or absorption at water/solution interface and prevents the coalescence, allowing the droplets growth through humidity absorption [134]. Another effect that avoids coalescence is the laminar flow of gasses passing in proximity of the drops. In fact, the evaporating solvent and the flowing air, together pass around each drop by thermo-capillary convection creating a laminar flux that hind the drop coalescence [123].

Resuming, the BF process is composed of many factors that act at the same time: surface tension and capillary forces controls the buoyancy and arrangement of the droplets; Marangoni convection induces convective fluxes, which encapsulate with a polymer layer each drop; convective motion, inter-capillary forces and external air fluxes control the movement and packaging of the drops. The complexity of these phenomena makes really hard to predict the resulting BF pattern starting from designed experiments with defined combinations of polymer and solvents.

4.5. Final stage

In the final stage, the drops diameter increases until reaching a critical value at which the thin polymeric layer between each drop is disrupted causing drops coalescence. At the same time, since this phenomenon occurs at the final stage of the BF process, with large part of the solvent evaporated, the increased viscosity of the solution slows down the entire process. When the solvent and water evaporation is completed, a polymeric surface patterned film remains on the substrate, with the final specific pattern depending on the defined variables of the process.

4.6. Effects of the process variables

The applications of the BF arrays depend on two main factors, the BF chemical composition and the final array impressed on the material surface. As described above, many materials can be used for the BF process and the many variables involved can be tuned in order to modify the final surface pattern. Many experimental variables can be used in the process and, despite many theoretical studies, it is still almost impossible to predict the final BF structure for a specific polymer-solvent combination. The critical factors have been identified in polymer and solvent nature, solution concentration and humidity. Other parameters can affect the process such as the nature of the substrate, the presence of surfactants to decrease the surface tension and the morphology of the substrate, but these contributes are minimal respect to the previous one. In general, many variables together can affect the same physical phenomenon and, at the same time, single variables can affect many of them.

Polymer nature. The main parameter that affects the BF formation for a specific polymer is the molecular weight (M_w). It has been demonstrated that there is an optimal range of M_w for regular BF formation [135]. An excessively low M_w leads to the formation of dispersed an irregular pores on the film surface, while an excessively high M_w hinder the water drops penetration

due to the high viscosity of the solution, resulting in films without pores [136]. The viscosity, which depends on the M_w, plays an important role in the process. Solutions with low viscosity cannot prevent the coalescence due to the weak polymer layer present around each drop. On the other hand, solutions with too high viscosity impede the drops sink. Inside the optimal range, M_w allows the formation of regular pores with monodisperse dimensions. Increasing the M_w inside the optimal range, the formation of pores with higher diameter were observed with an higher interspacing value [135,136].

Solvent nature. Density, surface tension and its temperature derivative, viscosity, thermal expansion and conductivity, thermo-dynamical affinity with the polymer, high vapor pressure, water immiscibility and high volatility are all fundamental parameters to take in consideration for the solvent choice in BF process [124]. The most used solvent are carbon disulfide and chloroform, but other studies demonstrated that also ethylacetate, tetrahydrofuran, dymethyl sulfoxide, dichloro methan, xylene, toluene, benzene and chlorofluorocarbons can be used [137]. The evaporation rate, with all the effects explained above, is an important factor that not only depends on the solvent nature. The BF process can be performed in static conditions, with a static humid environment, or in dynamic conditions, with a humid gas flow directed on the solution surface. The gas flow, usually air, can increase the evaporation rate of the solvent directing also the droplets deposition. The drops nucleation, diffusion and growth are time-dependent phenomena (eq. 1.1 and 1.2). The solvent evaporation can directly influence the three events because a fast evaporation increases the solution viscosity, hindering movement and growth. On the contrary, too slow solvent evaporation leads to drops coalescence. The gas flow, besides the solvent choice, can regulate the evaporation rate extending or shortening the complete solvent vaporization [126,137].

Solution concentration. The final pores size is directly proportional to the growth rate in the initial stage, which is influenced by the vertical temperature gradient created during the solvent evaporation. Low polymer concentrations lead to a high solution vapor pressure, which has as consequence an increase in ΔT and fast solvent evaporation. The final result, for solutions with a low polymer concentration, is surfaces with a bigger pores diameter respect to high concentrations where the diameter value is lower [124]. Another consequence of the modification of solution concentration is the compressive capability of the polymer layer between each drop. Decreasing the polymer concentration, drops can expand the diameter easier than a solution with a high concentration, resulting in pores with a bigger diameter [137]. Too high or too low solution concentrations inhibit BF formation. In the first case, the low polymer concentration is not able to contain droplets leading to a fast coalescence and no BF formation, while too high concentrations don't allow the drops penetration, resulting in final flat films [124].

Humidity. As the logic suggests, high humidity is fundamental for the BF formation. The process cannot happen when the humidity value is too low, but there is not a specific critical value at which the process suddenly starts. Generally it depends on the capacity of polymer to stabilize the water drops. The lowest value reported is 30% RH for a solution of PLGA and polyurethane [138]. Above a specific value, determinable for each polymer-solvent system, the increase in temperature leads to increase in pores size due to the difference in partial pressure of water vapor [135].

4.7. Combined Breath Figure method

Despite the complicated and concatenated physical phenomena involved, the BF process is one of the most fast, cheap and simple, compared to other techniques. It is applicable to a wide range of materials and the evaporation of the solvent, which is the time-consuming part of the process, takes from seconds to minutes. The many materials usable, combined with the different

obtainable topographies, can expand the application fields of the final surface porous materials. In recent years, the BF process has been modified in order to expand the potential of the patterned material. One example is the introduction into the system, of amphiphilic molecules with the ability to precipitate on the solution/water interface, exposing a functional groups on the pores surface allowing the specific surface functionalization [139]. The BF process is normally used to produce 2D porous films but the synthesis of 3D structures BF decorated are interesting under different point of views. For this reason, BF method was combined with electrospinning to create random or aligned fibers with a specific surface porosity present on each structure. The result is a mesh with a high surface area, nanoroughness, hierarchical structure and super hydrophobic behavior applicable in filtration, chemical analysis and biomedical applications [134]. For some application, a high chemical and physical resistance is needed where polymeric BF cannot be applicable. In the wide range of usable materials also some polysiloxanes have been used for the BF process, which represent the ceramic precursor in the Polymer Derived Ceramic (PDC) field. This combined technique concerns the formation of the BF pattern on materials convertible into ceramic through a pyrolysis step. Under specific conditions, the micropattern can be preserved allowing the formation of a ceramic surface with high corrosion and thermal resistance and with higher mechanical properties respect to the polymeric BF [140,141].

Experimental Section

1.   *Summary of the research*

1.1.   **Rationale**

Surface porous silicon-based ceramics are a class of materials with high mechanical, physical, biological, chemical and optical properties, which can be modulated modifying the chemical coordination in the silicon network or by changing the surface pattern. Nowadays different methodologies can be

performed driving the final ceramic chemical composition and the formation of a specific pattern. Despite this variety of methods, in many cases the techniques are really expensive and time-consuming forcing the application of two or more combined techniques to have the desired ceramic. Moreover, it is usually not possible to have different silicon-based ceramics starting from the same polymeric precursor. All the listed ceramics find an application in different fields but, one of the most promising, regards the application of SiON as implant coating material. Previous studies demonstrated the osteoinductive potential of Silicon Oxynitride (SiON) ceramics applied for implant coatings purposes. The principal reason for the application of this material is the ability to release Si^{4+} when exposed to the physiological environment. In fact, many studies proved the osteoinductive effects of silicon ions on osteoblasts and osteoprogenitor cells. Besides the promising results, the synthesis processes and the final produced material still present some disadvantages. In particular, plasma enhanced chemical vapor deposition, the most used technique used for the SiON synthesis, is a very expensive and time-consuming process, while doesn't allow to set a specific surface pattern and to control the film thickness. Moreover, the control of Si^{4+} needs to be regulated in order to release a specific amount of ions extended in time. A new fast and easy technique, called BF method, allows to synthesize surface porous films with different topographies simply varying the parameters involved in the process. Many studies demonstrated the possibility to decorate different materials, such as polymers, nanoparticles, organic and inorganic materials and biological molecules, with specific patterns, spacing from the typical honeycomb structure to multi-layer 3D porosity and other geometrical features [124]. The introduction of the combined BF method with the Polymer Derived Ceramics (PDC) allows to extend the application fields also where high mechanical properties and chemical-physical resistance are needed. In this study we propose a new method to obtain a surface patterned ceramic, with tunable pores size, using a UV-photo-crosslinkable alkoxy silicone, Loctite® 5248™, for the BF process. The evaluation of the variables effects on the final BF product

shows the possibility to control the final structure in terms of pores diameter, density, shape, film thickness, porosity degree and pores interspacing. In this way, many surfaces with specific topographies were obtained. Subsequently, all the pre-ceramic materials were pyrolyzed under ammonia atmosphere in order to induce the ceramic conversion. Finally, SiON ceramics produced in this way were evaluated for pattern preservation, chemical composition and biological activity. Schematically, the experimental work flow can be divided into three steps: Breath Figure process, heat treatments and ceramic characterization.
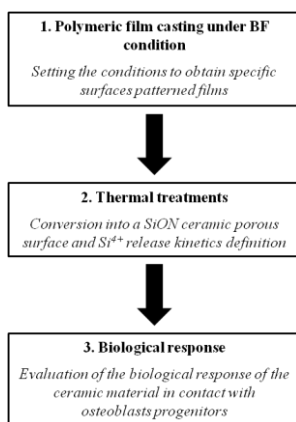

1. Polymeric film casting under BF condition

Setting the conditions to obtain specific surfaces patterned films

2. Thermal treatments

Conversion into a SiON ceramic porous surface and Si^{4+} release kinetics definition

3. Biological response

Evaluation of the biological response of the ceramic material in contact with osteoblasts progenitors

Figure 5 Schematic representation of the proposed work flow

The research themes were developed as described below following figure 5:

1.   **Variables effect evaluations in the BF process using a photo-crosslinkable alkoxy silicone.** Variables effects that most affect the final product were studied in order to finely control the process and pattern the resultant surface with a specific geometry. The different surface patterned materials were characterized determining the surface morphology.

2.   **Set up of heat treatments that allows both the ceramic conversions and the chemical modifications of the silicone.** Oxidative

ammonia and air, and inert nitrogen atmospheres were tested to evaluate the chemical modifications. All the samples were characterized for chemical modifications and surface porosity preservation.

3.   **Biological evaluation of the pyrolysis products**, taking in consideration and comparing different surface porosity to assess silicon ion release capability, cells adhesion, morphology proliferation rate and the modulation of enzymes related to the bone healing process.

The obtained results demonstrate a new way to synthesize SiON surface porous materials with tunable pores geometry using a fast, easy and highly controllable technique. The materials obtained have the potential to be used as implant coatings in order to induce bone apposition and long-term implant fixation.

1.2.   Breath Figure process

Loctite$^{®}$ 5248$^{™}$ is a medical grade, UV-photocross-linkable alkoxy silicone already used as sealant for tooth root fixation. It has been choice for two main reasons: the SiO_2 backbone, which can be heat treated without big morphological modifications, and the photocross-linkable nature, which allows an in-depth study of the BF process with an increase in mechanical properties. The material nature allowed us to "freeze" the BF process in every moment simply exposing the solution to UV-light in order to understand the contribution of each stage in the final result.

The main process variables affecting the final film pattern were evaluated and are listed in Table 4. In this part we evaluated synthesis of BF alkoxy silicone films with tunable pores geometry, in terms of pores shape, density, diameter, depth and order. To deeply understand this process, all the variables were tested, alone or in combination, evaluating their effects on the final pattern.

Table 4 List of the investigated values. Adapted from [142]

Variables	Investigated Values
Precursor concentration	From 0,5% to 20% w/w
Solvent	Ethyl acetate, Chloroform, Dichloro methane, Dimethyl Sulfoxide, Hexane, Carbon disulfide
Surfactant	0,1 to 100% w/w of the silicone (HLB = 1 ÷ 6)
Substrate	Quartz, Glass, Poly ethylene terephthalate, Mica, Water and Glass treated with oxygen plasma
Flow Rate	0,1 to 1,6 L7min
Pre-Exposure Time	0 s to 20 mins
Vapor Temperature	25°C to 75°C
Humidity	60% to 99% RH
Spin-Coating	Round per minute: 80 to 4000 RPM Time: 3 to 20 s Acceleration: 150 to 1500 RPM/s
Conformal-Coating	Water removal speed from 1 ml/min to 5 ml/min

1.3.   Heat treatments

To be used as implant coatings, the chosen material needs to have a high corrosion resistance, potential bioactivity and a good adhesion to the coated metal. For these reasons, we decided to convert the silicone BF in a SiON following the PDCs route. The pyrolysis step, under ammonia atmosphere, allows the modification of the pre-ceramic chemical structure through combustion of the organic carbon, present in the -SiO_2- chain, and nitridation of the network. To induce these two reactions, the temperature was set at 900°C for 1 hour. After the treatment, the obtained ceramic materials were characterized for morphology preservation and chemical composition.

1.4. Ceramic conversion

The last part was dedicated to the bioactive potential evaluation through the analysis of the ion release and the biological response of cells from materials with different porosities. The silicon ion release was tested and quantified on different pores diameters. After that, the influence of pores structure and ion release were biologically assessed. Human Mesenchymal Stem Cells (hMSCs) were seeded on ceramics with three different pore sizes and evaluated for adhesion, morphology, proliferation rate and metabolic and alkaline phosphatase activity. The results were compared with the one obtained from a flat SiON ceramic and Titanium-6-Aluminum-4-Vanadium (Ti6Al4V), widely used as implant material.

2. *Materials and Methods*

2.1. Breath Figure process

Solvents and surfactants used in the process were pursued by Sigma Aldrich (USA) and are listed in Table 4. The alkoxy silicone Loctite® 5248™ (AG & Co, Germany, Henkel) was used as received and dissolved in different solvents to obtain concentrations between 0.5% and 20% w/w. The BF process was performed in special chamber built following the description of Maniglio *et al* [143]. Briefly, an aluminum chamber, equipped with a UV-Light transparent PLEXIGLAS Solar®, was filled with humidity using a N_2 flow forced in a gas bubbler. The flow was controlled using a flow meter, ranging between 0,1 and 1,6 L/min. The UV-crosslinking was induced exposing the solution to a UV LED Spotled 365/15 curing equipment (Photo/Electronics srl, Italy) emitting at 365 nm. The exposition was performed at different time-points after the solution casting. All the surfactants were used as-received and dissolved in the starting solution. The combined spin-coating in BF regime was performed using a H6-15 spin coater (Laurel Technologies, USA) varying rotation speed and acceleration. Conformal coating was performed on as received Ti6Al4V disks and screws (Eurocoating, Italy).

The morphological characterization for all the samples was performed using optical microscopy and scanning electron microscopy (Zeiss Axiotech 100 and Zeiss supra 40) after Pt/Pd coating. Pores diameter and statistics were calculated using ImageJ and OriginPro Lab.

2.2. Pyrolysis step

The ceramic conversion was induced in a silica tubular furnace (Thermo Scientific Heraeus) at 900°C for one hour with a ramp of 5°C/min both for heating and cooling phases. To perform the nitridation, flowing ammonia was used during the treatment. Morphology and structure preservation were evaluated with scanning electron microscopy as described above. The amorphous ceramic conversion was evaluated through X-ray diffraction spectra using a Bruker D8 Advanced X-ray diffractometer with glancing angle Bragg-Brentano geometry using Cu kα radiation λ=1,5418 Å at room temperature, range of 20-80˚ with a 0,02˚ step size and a dwell time of 1 second. Chemical composition and atomic bonding state were evaluated using X-ray photoelectron spectroscopy with a Scienta-Gammadate ESCA 200 equipped with a monochromatized Al kα X-ray source 1486,6 eV.

2.3. Ceramic characterization

Silicon ion release of materials with different surface patterns was evaluated using Inductively Coupled Plasma – Optical Emission Spectroscopy (ICP-OES, ICPE-9000, Shimadzu Multitype ICP Emission Spectrometer) with each sample immersed in alpha-MEM (Minimum Essential Medium Eagle with Alpha Modifications, Sigma-Aldrich) at 37°C and 5% CO_2. hMSCs (Lonza, Switzerland) were maintained using DMEM/Ham's F-12 1:1 (Sigma-Aldrich) with 10% of FBS and 1% Penn/Strep (Invitrogen, Carlsbad, CA). Cells were cultured and maintained at 37°C and 5% CO_2 with the medium changed every 48 hours. All the tested samples were sterilized with autoclave. A cell seeding density of 10^4 cells/cm^2 was used for the confined drop method.

Confocal Microscopy.

Cells adhesion, morphology, proliferation and distribution were evaluated using a Nikon A1 confocal microscopy (Nikon Instruments, Amsterdam, The Netherlands) after fixation in formaldehyde 4% in PBS and permeabilization with Triton-X 0,1% in PBS. Nuclei and cytoskeleton were stained with DAPI(4',6-diamidino-2-phenylindole dilactate, Invitrogen, Oregon, USA) and Oregon Green® 488 Phalloidin (Molecular Probes, Oregon, USA). was evaluated with Alamar Blue® (Invitrogen, Oregon, USA) following the manufacturer's guidelines.

Metabolic Activity.

Cells metabolic activity was determined using Alamar Blue® reagent. At each time-point, culture medium was removed and replaced with 1 ml of new medium with 10% of Alamr Reagent. After 1 hour, 100 µl of supernatant was collected in triplicates and the fluorescence emission at 590 nm was read using a microplate reader (Spark 10M, Tecan, Austria) after excitation at 560 nm.

Cell Proliferation.

The proliferation rate was quantified using Quant-iT PicoGreen® dsDNA Assay Kit (Invitrogen, Molecular Probes, Oregon, USA) following the manufacturer's guidelines. For each time-points total DNA was collected using 500 µl of Triton-X 0.05% in PBS after rinsing with PBS. After an incubation of 30 minutes, the obtained solution was sonicated for 20 seconds with a Virsonic ultrasonic cell disrupter (Virtis, Warmister, PA), then the fluorescence emission of the PicoGreen-DNA complex was measured with a microplate reader. The fluorescence intensity was interpolated with a calibration curve built using the DNA standard provided, correlating the fluorescence intensity with the DNA concentration.

Alkaline Phosphatase Activity.

The Alkaline Phosphatase Activity (ALP) modification was calculated using ALP assay (Fluorimetric, Cambridge, UK) following the manufacturer's instructions. At each time points, culture medium was removed and each sample was washed three times in PBS. Cell lysate was collected, as described previously, using 500 µl of Triton-X 0.05% in PBS incubated for 30 minutes. After the incubation time, the solution was sonicated for 20 s. ALP concentration was measured by fluorescence intensity using a microplate reader (excitation at 360/35 nm, emission at 430 nm) and the obtained value was interpolated with a calibration curve built using the provided standard.

3. Results and Discussion

3.1. Breath Figure process

As described in previous paragraphs, we tested all the variable combinations in the BF process to investigate the effects on the final pattern. Each variable influences a specific behavior of the process, and so, of the surface pattern in terms of pores diameter, shape, density, organization, order and depth. Here we report the results for: time before UV-exposure, precursor concentration, surfactant presence, conformal coating, spin-coating and other significant results.

3.1.1. Time before UV-Exposure

Using a UV-crosslinkable material, such as Loctite® 5248™, the process can be stopped in each stage simply exposing the solution to the UV light as described by Maniglio *et al* [143] in a previous work. The curing time and depth of the material are compatible with this purpose.
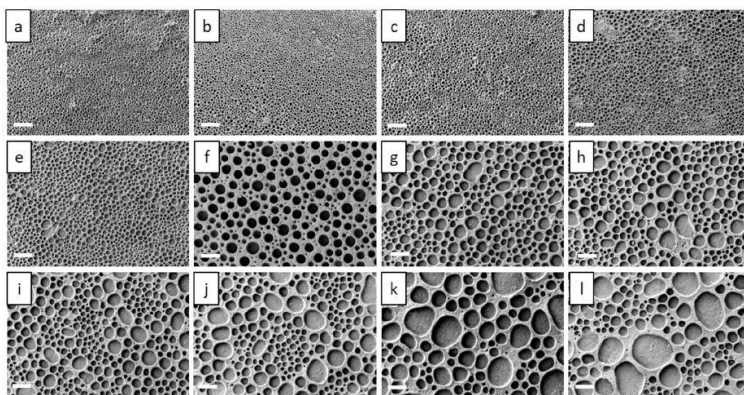
Figure 6 Scanning electron microscopy of samples obtained with silicone concentration of 5% (from a to i), 4% (j), 3% (k) and 2,5% (l). The exposure times used for the samples production are: 1' (a), 2' (b), 3' (c), 4' (d), 5' (e), 6' (f), 7' (g), 8' (h), 9' (i), 10' (j), 11' (k), 12' (l). Scale bar 100μm. Picture from Carlomagno C *et al* [142].

The experiment was performed waiting specific times between solution casting and UV exposure. Results of increasing pre-exposure time, from 1' to 12' (minutes), and precursor concentration, from 5% to 2,5%, are reported in figure 6. A linear increase of the pores diameter was observed using a silicone concentration of 5% and increasing the pre-exposure time from 1' to 9' (Fig.6 a-i). Higher the pre-exposure times result in a no further expansion of pores from samples prepared with that concentration (Fig.6 i), probably due to the solvent evaporation and consequent increase in viscosity. To have higher pores diameter, we tried to decrease the solution concentration to 4%, 3% and 2,5% increasing, at the same time, the pre-exposure time. This approach allowed us to expand the pores diameter up to 200 μm sacrificing the homogeneity of the pores distribution (Fig.6 j, k, l). The main phenomena determining the ores growth are the continuous absorption of humidity from the environment and the drops coalescence during the process. Coalescence, in this system, occurs principally when the number of drops on the solution surface is really high and the limited available space

induce a pressure between each drop present on the liquid surface. In this case the principal barrier to avoid coalescence is the compressed polymeric layer between each drop, in which compression resistance is dependent on the starting polymer concentration. Increasing polymer concentration, the compression capacity is higher, allowing the growth through humidity absorption, and avoiding the droplets coalescence, resulting in smaller drops diameter. On the other hand, a decrease in polymer concentration leads to a lower compression capacity making the drops coalescence easier [144].
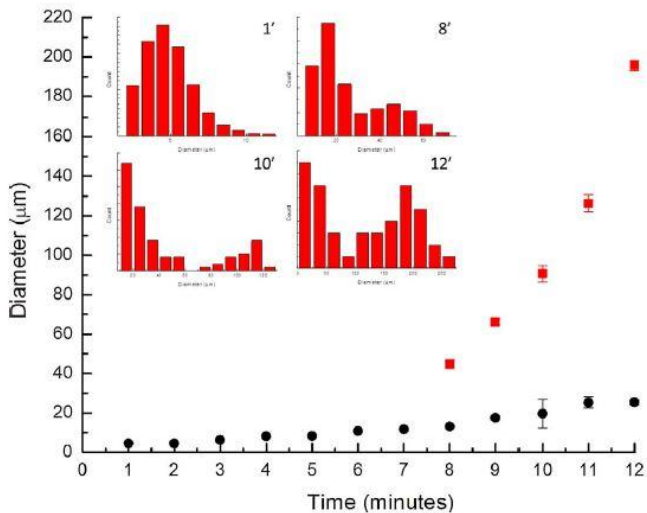

Figure 7 Relationship between pre-exposure time and pores diameter (dots and squares) using a concentration of Loctite® 5248™ of 5% (1' to 9'), 4% (10'), 3% (11') and 2,5% (12'). Graphs show the pores diameter frequency counts for the indicated pre-exposure times [142].

Figure 7 shows the relationship between pre-exposure time increases and pores diameter. From 1' to 7' (Fig. 7 1' to 7') the diameter grows uniformly. Starting from minute 8', two main peaks in the diameters concentrations are observable (Fig.7 8'; graph 8'). This phenomenon can be explained with the continuous formation of new droplets on the solution surface (Fig.7 circles)

and the absorption of humidity from the environment, which allows an expansion of drops diameter (Fig.7 squares). Further increase in pre-exposure time together with solution concentration decrease, sharpens the expansion effect. This phenomena is due to the coalescence of the droplets during the process, resulting in pores with a higher diameter (Fig.7 10', 11' and 12' squares) and the double trend of droplets growth.

3.1.2.   Precursor concentration

Figure 8 shows the patterns produced from different concentrations of Loctite® 5248™, keeping constant all the other process variables. When a solution concentration of 0,5% w/w is used, the result is a pattern with interconnected pores and with a high random distribution (Fig. 8 a) generated from a massive drops coalescence. In fact, as explained in previous paragraph, a low concentration of precursor cannot avoid drops coalescence caused by the excessively low solution viscosity.
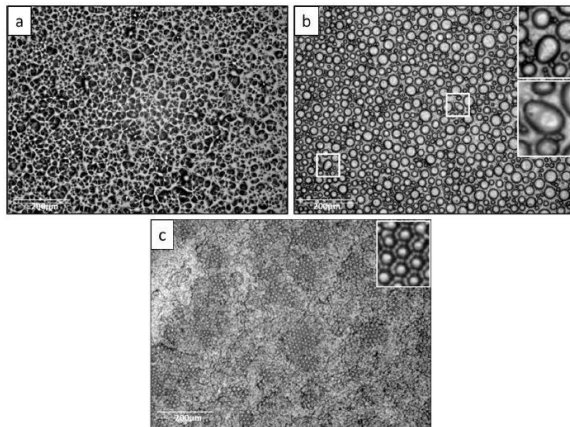

Figure 8 Optical microscopy of samples prepared with different concentration of Loctite® 5248™: 0,5% w/w (a), 5% w/w (b) and 15% w/w (c). Scale bar 200 μm

Increasing the concentration up to 5% and 15% (Fig. 8 b and c) resultant pores are distributed in a more organized pattern accompanied with a diameter decrease. The film resulting from 5% solution concentration (Fig. 8 b and Fig. 9 a) presents two families of pores ranging from $16,5 \pm 0,3$ μm and $31,8 \pm 0,1$ μm, with a pores depth of $11 \pm 0,5$ μm (Fig. 9 a inbox). The bimodal distribution is reasonably due to the coalescence of droplets (Fig. 8 b inbox) and to the continuous formation of new droplets. Increasing the concentration up to 15%, two distinct regions can be observed: one with the typical high-packed honeycomb structure, with a pores diameter of $6,6 \pm 0,1$ μm, and the other one not presenting any specific organization (Fig. 8 c). A possible explanation is that the concentration gradient produced from the casting method can determine the appearance of regions with different polymer viscosity.
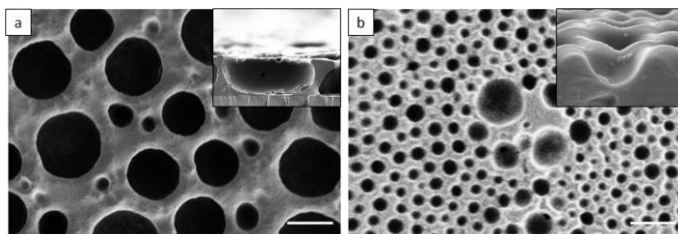

Figure 9 Scanning electron microscopy of BF films made with a Loctite® 5248™ concentration of a) 5% and b) 15%. Inbox of each picture shows the vertical section after liquid nitrogen break. Scale bar 30μm

In regions where viscosity is too high, water cannot penetrate the surface so that BFs cannot generate (Fig. 8 c), while, in regions where the viscosity is reduced, water can penetrate and a regular pattern is formed, even if drops penetration is lower with respect to the film prepared from 5% solution (Fig. 9 b inbox). We also observed that, with solution concentration of 20%, BF pattern couldn't form.

Observing morphologies of films as in the sequence proposed with Fig.6 j, k, l and Fig. 9 a and b, it is possible to describe general trend: the increase in polymer concentration leads to a decrease in pores diameter. A possible explanation for this phenomenon can be find in Henry's law, which states that the vapor pressure of a solution is lower than the one of the same pure solvent:

$$P_{sol} = P_0(1 - X_b)$$

[1.9]

Where P_{sol} and P_0 represent respectively the vapor pressure of the solution and of the pure solvent and X_b is the mole fraction of the solution. The difference in temperature between the atmosphere and the solution surface ($\Delta T = T_{atm} - T_{sol}$) decreases together with the evaporation rate of the solution and also with its vapor pressure. During the initial stage of the BF process, the drops radius variation in the time (dR/dt) increases in a proportional way with the $\Delta T^{0.8}$ of the system:

$$\frac{dR}{dt} \approx \Delta T^{0.8}$$

[2.1]

Consequently, a higher solution concentration leads to a lower vapor pressure and therefore to a lower ΔT, which results to smaller pores diameter and vice versa [145,146].

3.1.3. Surfactant presence

As described in previous works, the presence of surfactants in the solution decrease the surface tension at the water/solution interface [147]. The disposition of these amphiphilic molecules, with the hydrophilic domain

oriented to water phase and the hydrophobic one to the solution, facilitates the penetration of droplets in the solution surface, as showed schematically in figure 10. The importance of the surfactants use is not only in the facilitation of the BF process, but also in the possibility to functionalize the pores surface with a specific functional group exploiting the amphiphilic domain of the molecules.
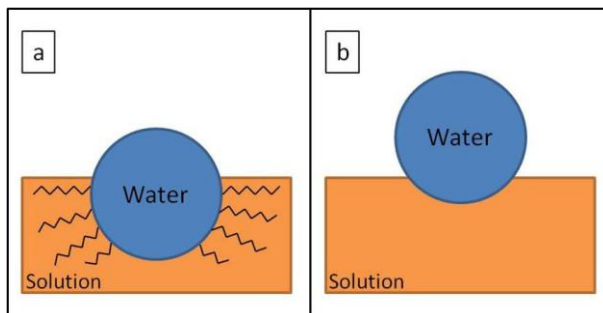

Figure 20 Schematic representation of the a) surfactant assisted BF process and b) the normal one using solutions with the same concentration

In our work we tested amphiphilic molecules with a Hydrophilic/Lipophilic Balance (HLB) from 1 to 6, identifying two molecules particularly effective for BF formation and pores surface functionalization: Labrafac® PG (HLB=1) and 11-Mercapto-1-Undecanol (HLB=5.5). The first molecule was tested to evaluate the surface tension decrease and consequent BF formation facilitation, while, the second one was used to expose thiol groups on the pores surface for the potential functionalization of pores surface with other structures (i.e. gold nanoparticles)
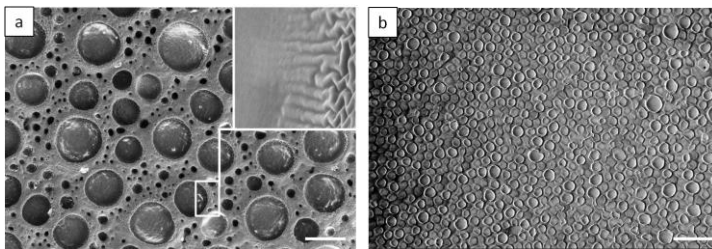
**Figure 11 Scanning electron microscopy of BF made with 10% w/v of Loctite®
5248™ a) with the addition of 5% w/w of the precursor in Labrafac® PG
(HLB=1) and b) without the surfactant addition. In box a) shows a high
magnification image of the pores edge. Scale bar 30μm.**

In figure 11 are shown the results of two BF patterns made with the same
precursor concentration, 10% w/v of Loctite® 5248™, with (Fig.11 a) and
without (Fig.11 b) the surfactant presence in the starting solution. Due to the
high solution concentration and the resultant viscosity, water drops cannot
penetrate the solution surface during the BF process resulting in the
formation of superficial drops marks, as visible in figure 10 b. Adding the
surfactant in the starting solution it is possible to observe the formation of a
BF array, despite the high solution concentration. The pores depth for the BF
made with the introduction of the surfactant is 10μm ± 0,5μm and is not so
different from the one calculated previously (Fig.9a inbox). Without
surfactant, the solution concentration limits the drops penetration showing a
resultant pores depth of 1μm ± 1,2μm. Another effect that can be observed is
the formation of microstructures on pores edges (Fig.11 a inbox), which are
not present in samples produced without surfactant, probably due to the
aggregation of the molecules into supramicellar structures [148]. In this case,
the BF decoration was made on solution too viscous to be patterned with the
normal BF process. For this reason, the surfactant assisted BF process can be
a potential method to increase the ranges of concentrations at which BF can
occur, to better control the pores depth and, also, to induce the formation of
a second order pattern on pores edges. This result could be exploited for
realizing substrates usable for Surface Enhanced Raman Spectroscopy

(SERS), where the functionalization of the surface, with Raman active particles, and a high surface area are required.

3.1.4. Conformal coating

For the design of an implant coating, over the synthesis process, it is fundamental to evaluate the deposition on the metal prosthesis. As described above, many techniques are able to synthesize the coating directly on the metal surface with many problems caused by pattern resolution, material attachment, delamination and others. The BF process allows to create a controlled porosity generally on flat substrates with some exception. Some study reported the formation of BF films on 3D materials using solvents with a low T_g and taking advantage from the polymer plasticization by the solvent [124]. Limitations of this approach are in the size of the material that can be coat, in fact in all the reported works, only materials in the micron range and with a regular shape have been coated. To overcome this problem, we proposed a new BF process performed using as substrate, the flat surface of water.
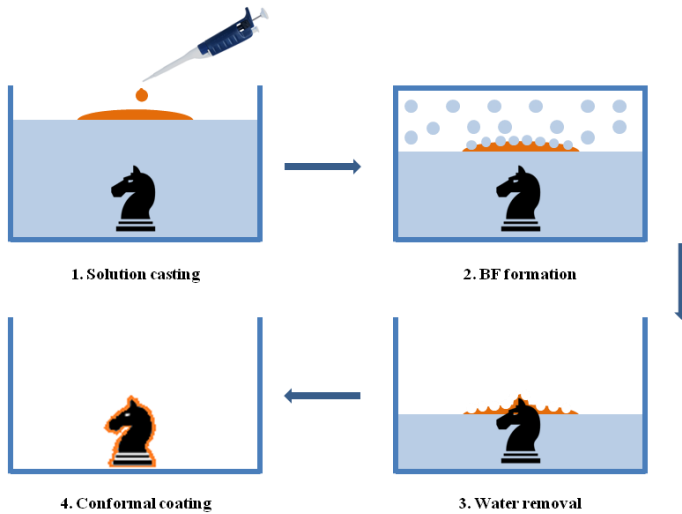
Figure 12 Schematic representation of the water assisted BF casting. 1) Solution casting on the water surface with the object immersed, 2) BF formation, 3) gradual water removal, 4) 3D objects conformal coating

In figure 12 the schematic representation of the proposed process is shown. Briefly, the 3D object to cast is immersed in water and the BF starting solution is casted on the water surface. The solution floats on water due to the hydrophobic nature of the solvent. After the casting step, a humid environment is created through flowing nitrogen and/or with the water below. In this way a floating surface porous polymeric layer is created. A gradual water removal allows to slowly coat the 3D object till a complete conformal coating. To test this process, we tried to coat a copper wire, a pipette tip and a Ti-6-Al-4-V screw used for dental implants.
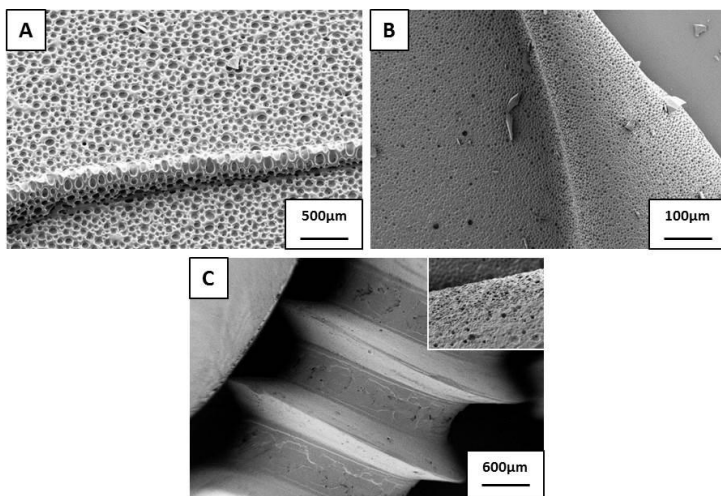
Figure 13 Scanning electron microscopy of BF coatings on a) copper wire, b) pipette tip and c) Ti6Al4V screw (in box higher magnification).

Figure 13 shows the results for the conformal coatings applied to a copper wire (Fig.13 a), to a pipette tip (Fig.13 b) and to a Ti-6-Al-4-V screw (Fig.13 c). The water removal speed was 10ml/min and was kept constant for all the samples. The slow and gradual water removal allows the film adhesion on all the material structures and is fundamental to avoid the "curtain effect" that is the result of a imperfect adhesion. For the BF process a solution concentration of 5% w/v with a pre-exposure time of 6' was used. If compared with results obtained when the solution was casted on a flat surface (Fig. 7), the main diameter shows an increase probably due to the relaxed conformation when the film floats on a liquid substrates. This phenomenon can be explained with the evaporation starting point when the solution is casted on a solid flat substrate. In this case the evaporation starts from the external part of the solution, which is the first region that solidifies due to the rapid solvent evaporation. This outer layer compresses the central solution part making difficult the drops expansion promoting the coalescence instead of the diameter increase. When the solution is casted on water, the solvent evaporation starts uniformly from the entire surface,

60

promoting the drops expansion by humidity absorption instead of the coalescence. For this reason pores present a higher diameter if compared with the one obtained using the same conditions on a solid substrate [149,150].

3.1.5. Spin-coating

Spin-coating is a technique in which a solution is casted on a rotating substrate in a controlled atmosphere. This method is widely used to obtain very thin coatings on flat surfaces. Generally, the material is deposited at the center of the substrate, placed on a speed controlled rotating stage. The sample is put in rotation so that centrifugal force induces the uniform spreading of the solution on the surface. Rotation continues until a desired thickness and a uniform coating is obtained. When the solvent used for the material deposition is highly volatile, evaporation occurs during the spreading, so, if the spin-coating is performed in a humid atmosphere, BF patterns can form (Spin-coating BF method [151]).

We have tested this technique using 5% w/v Loctite® 5248™ solution in ethyl acetate, casted on a glass substrate (microscope coverslips) before starting the rotation (static approach). The chamber was saturated with a humid nitrogen flow to reach a RH of ~95%.
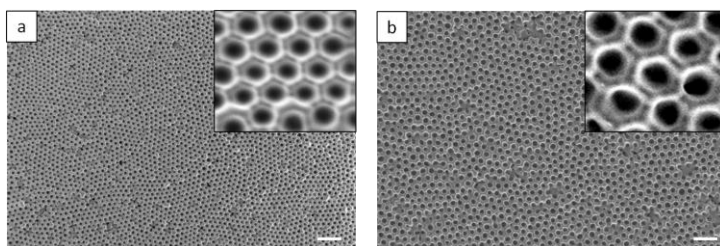

Figure 14 Scanning electron microscopy of SC-BF samples obtained with a) rotation speed of 200 rpm and b) 140 rpm, both for 5 seconds. In boxes show the high-resolution image for a single high-packed cell. Scale bar 20μm

As shown in figure 14, the combined SC-BF method allows the formation of the typical high-packed honeycomb pattern on the film surface (figure 14

inboxes). With this geometry, each pore is surrounded by other six pores in a hard-sphere like interaction. Pores show a narrow mean diameter size of 5,8 $\pm$ 0,2 µm and 6,4 $\pm$ 0,1 µm for the surfaces produced using respectively 140 and 200 rpm. The rotational speed influences the quantity of material left on the substrate before starting the condensation of water droplets. Thus, is possible to control two main characteristics of the final material as described in literature: the overall surface thickness and pores arrangement [151,152]. The formation of a high ordered pattern is probably due to the elimination of the concentration gradient present using the normal deposition method. Dropping the starting solution on a solid substrate, the liquid forms a drop with a semi-elliptical shape depending on the substrate surface energy that influences the overall wettability (Fig.15a).
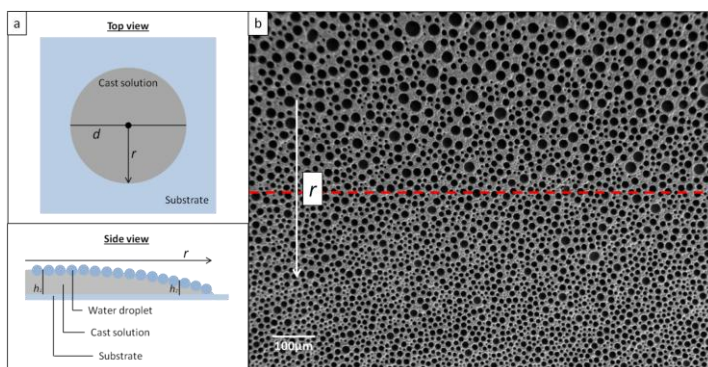
Figure 15 Representation of the concentration gradient effect created during the normal casting BF process. a) Schematic representation of the solution surface from the up section (top, r=radius; d=diameter) and the vertical section (down, h_1=height of the solution in the center; h_2=height of the solution in the edges). b) Scanning electron microscopy of a BF film showing the differences in diameter following the radius (r).

This phenomenon can be highly reduced, but not completely eliminated, increasing the substrate wettability through deep cleaning or spreading methods including exposition to O_2 atmospheric plasma, immersions in piranha solutions or using the spin-coating technique [151].

The main effect of the semi-elliptical shape is schematically represented in figure 15. The limited spreading of the drop creates regions of solution with a lower height (outer region, figure 15 a, h_2) respect to other regions (inner regions, figure 15 a, h_1). The evaporation of the solvent is faster on the edges (Fig.15a h_2) giving to the formed water drops less time to increase their diameter respect to the center of the liquid phase (Fig.15a h_1). As result, in the final BF film, pores possess a diameter gradient that increases moving radially to the center of the sample (figure 15 b, red line) [151,153]. This effect can be avoided using the SC-BF method, which results in a homogeneous pores diameter distribution on the entire film surface. In this process, the substrate rotation induces the solution spreading in a uniform way together with the removal of the solution in excess. At the same time, the solvent evaporation starts homogeneously on the surface driving the uniform drops growth. A slight increase in pores diameter was also observed decreasing the rotation speed, probably, due to the limited solvent removal and elongated evaporation time, which gives to drops more time for the diameter expansion [151].

3.2. Heat treatments

All the BF films underwent heat treatments to induce the ceramic conversion. Three different atmospheres were tested for the conversion of the precursor in different silicon based ceramics. In particular the pre-ceramic BF were treated at 900°C for 1 hour under air, nitrogen and ammonia in order to obtain respectively silicon dioxide, silicon oxycarbide and silicon oxynitride. Also these materials have been proposed as implant coatings for, respectively, middle-ear and heart valves prosthesis [31,154]. Once more, the surface porosity plays a fundamental role and the possibility to produce three different surface porous ceramics from the same precursor is of great importance under the production point of view. The modifications of the chemical composition during the ceramic conversion increase the physical, chemical and mechanical properties of the material introducing at

the same time also specific functions. For example, it has been demonstrated that SiON ceramics are able to release osteoinductive ions when exposed to the physiological environment [35]; SiO_2 is widely used for the easy functionalization of the silanol exposed groups [31], while SiOC present an enhanced anti-coagulant activity when in contact with the blood [32].

3.2.1. Air, Nitrogen and Ammonia

After the BF formation, all the silicone surface porous structures underwent to ceramic conversion, through heat treatments, under different flowing gasses, in particular air, nitrogen and ammonia.
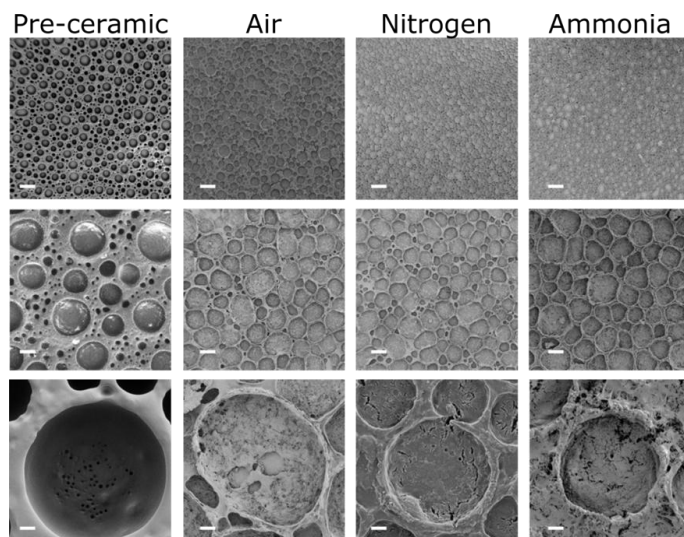
Figure 16 Scanning electron microscopy of alcoxysilane precursor (Loctite® 5248™) and the three ceramics obtained, with three different degrees of porosity [142]. Scale bar 10 μm.

Figure 16 shows the SEM images of the ceramic materials obtained after conversion in air, nitrogen and ammonia, starting from the correspondent pre-ceramic BF. As expected, all the materials preserved the surface porosity for all the used atmospheres, with minimal changes in pores diameters, reasonably due to the silicone shrinkage. The three porosity degrees were

obtained using different concentrations of Loctite® 5248™, respectively 3%, 5% and 7% for the higher, medium and smaller pores diameter. A preliminary visual inspection of the samples treated in air and ammonia showed the occurred organic carbon combustion due to the white color of the bulk samples [155]. Otherwise the material treated in N_2 atmosphere, appear black, which indicates the presence of free carbon inside the Si-O network [156].
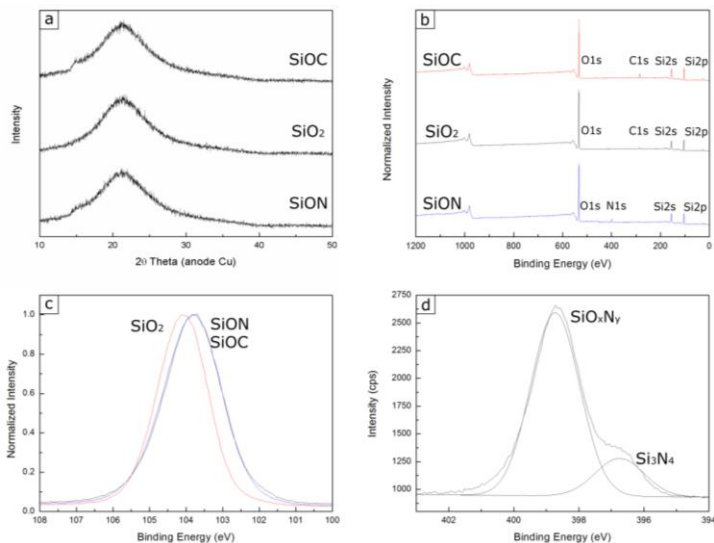
Figure 17 a) X-ray diffraction patterns and b) X-ray photoelectron spectroscopy survey of the ceramic materials. C) XPS Si2p spectra of the ceramics and d) N1 XPS signal of the material treated under ammonia flow [142].

The amorphous state of the treated samples were tested through XRD analysis (Fig. 17 a). The broad 2theta peak, located at ~20°, common to all the tested samples, is typical for the amorphous Si-based ceramics pyrolyzed between 800 and 1000 °C. This peak indicates that the SiO_2-based network dominates the diffraction patterns [142]. Materials chemical composition and specimen coordination were investigated through XPS analysis (Fig. 17 b, c and d). Figure 17 b shows the survey of the ceramic materials with peaks relative to Si, O, C and N presence. SiO_2 and SiOC spectra show only the

65

peaks of Si, O and C as expected, with the intensity of the C related peak with a lower intensity for the SiO_2 indicating that the air treatment induces carbon removal by combustion. Ammonia treated sample shows only the peaks relative to Si, O and N, indicating the complete carbon removal and the occurred nitridation [157]. The chemical nature in the ceramic materials was investigated acquiring the High Resolution Si2p and N_2 XPS spectra (Fig. 17 c and d). The Si2p peak of the material treated under flowing-air is centered at 104.1 eV, while the other two samples show a peak at 103.7 eV. The SiO_2 peak obtained is typical for the silica glass, confirming that the final material is a silicon dioxide. Shifts to lower binding energies indicate that Si shares a bond with C in SiOC and with N in SiON, respectively [158]. The N_2 s signal reveals the coordination of nitrogen in the Si-o network (Fig.17 d). The main component at 399,5 eV indicates the involvement in a silicon oxynitride unit, while the shoulder at 396,5 eV refers to the silicon nitride environment (Si_3N_4).

3.3. Ti6Al4V coatings and Silicon ions release

The SiON coatings with three different degrees of porosity were synthesized starting from 3%, 5% and 7% w/v silicone solutions in ethyl acetate. As solid substrate for the BF process, Ti6Al4V disks were used (diameter: 14 mm, thickness: 4 mm, surface area: 1,54 cm^2). To obtain a uniform porous coating, 80 µL of each solution was casted on the disks into a humid environment (RH ~ 95 %) and, after 8 minutes of exposition, the UV Led was turned on to fix the structure. The flat coating was obtained through solvent casting of a 5% w/v solution in a dry environment and used as a control group. The obtained materials are shown in figure 18. The coating made with the higher solution concentration (Fig.18 B) shows the lower diameter dimension, with a value of 13.1 ± 0.2 µm (small porosity) (Fig. 18 E).
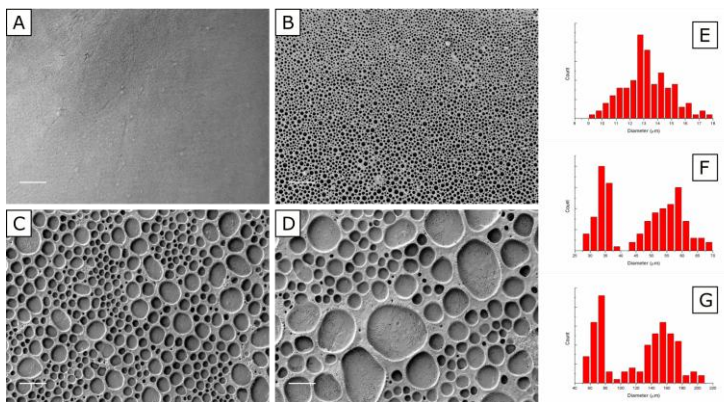
Figure 18 Scanning electron microscopy images of A) flat material made with 5% of Loctite® 5248™, B) BF made with 7% of Loctite® 5248™, C) BF made with 5% of Loctite® 5248™ and D) BF made with 3% of Loctite® 5248™. Scale bar 100 µm. Graphs show the diameter frequency count for E) 7%, F) 5% and G) 3% of Loctite® 5248™.

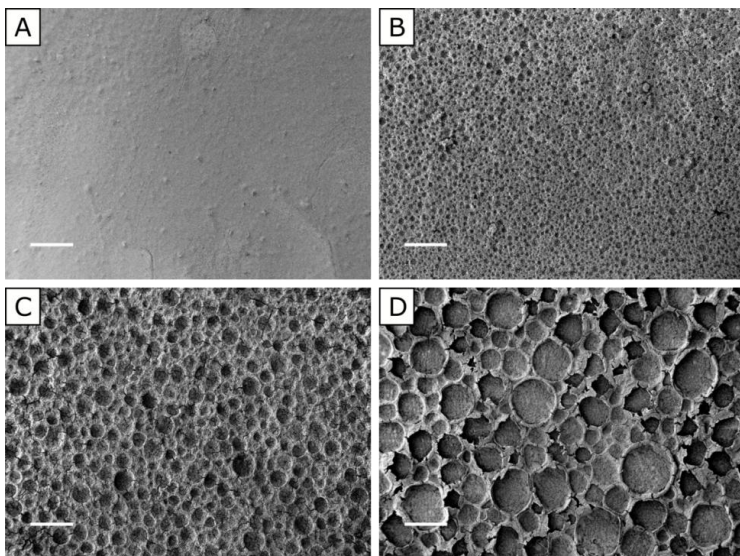**Figure 19 Scanning electron microscopy of A) the flat material and of BF made with B) 7%, C) 5% and D) 3% of of Loctite® 5248™ treated under ammonia atmosphere. Scale bar 100 µm. Adapted from Carlomagno *et al***

As explained in previous results (Fig.7), a decrease in concentration leads to the formation of a bimodal pattern due to the lower solution viscosity allowing a easier coalescence and new drops condensation [142]. Using the 5% solution, a mean pores diameter of 34.4 ± 0.3 μm and 58.8 ± 0.6 μm was obtained (medium porosity), while, decreasing further the concentration up to 3%, the diameter size increase to 71.3 ± 1.3 μm and 155.0 ± 1.6 μm (large porosity) (Fig.18 F and G). The flat material shows a uniform surface without the presence of microporosity. After the BF process, all the materials underwent pyrolysis in ammonia atmosphere (900 °C for 1 hour) in order to remove the organic carbon and to perform the nitridation of the Si-O network. Figure 19 shows the result of the heat treatment on the pre-ceramic materials. The micrometric porous structure was not affected by the treatment preserving the original patter. The pores diameters were conserved with no significant variations. To assess the ceramic conversion, chemical modifications and amorphous/crystalline state of the samples, XPS and XRD analysis were performed (Fig.20). As with the previous characterization, in the ceramic material, the XPS peak relative to the C presence completely disappears, substituted by the peak relative to N (Fig.20 A). The nature of N coordination inside the Si-O network was investigated analyzing the Si2p and N1s spectra revealing that N is present into SiO_xN_y and Si_3N_4 forms (Fig.20 B and C). In the same way, the heat treatment at 900 °C doesn't allow the formation of a crystalline structure, leading to the formation of an amorphous state (Fig.20 C).
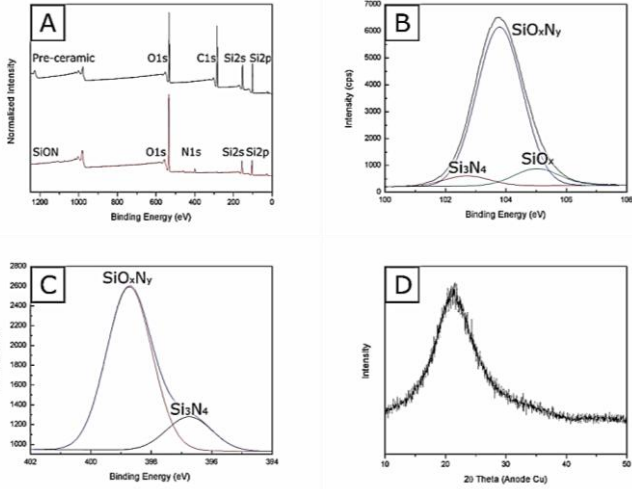
Figure 20 A) XPS analysis results for alcoxysilane (Loctite® 5248™) and the SiON ceramic. **B)** Si2p and **C)** N1s of SiON BF. **D)** XRD pattern of the ceramic material.
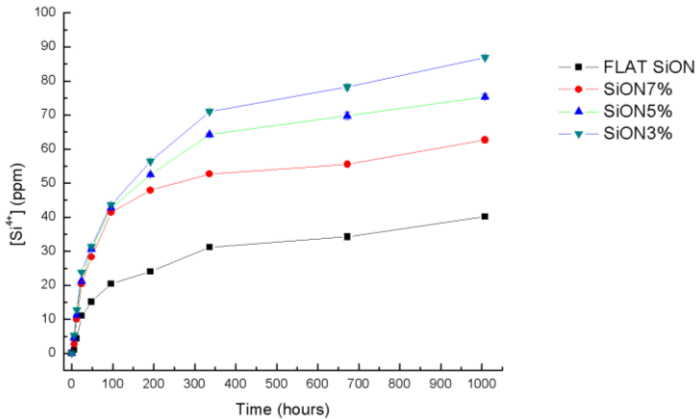

Figure 21 ICP-OES analysis of the Si^{4+} released from flat SiON (black squares) and ceramic BF made with 7% (red circles), 5% (blue triangles) and 3% (green triangles) of silicone concentration.

The Si-based ceramic amorphous state is fundamental for the interactions with the environment. As described in previous paragraphs, the ion release reaction starts in the -Si-OH specimen where O is not coordinated with other Si atoms (Table 2). This is an essential condition for the ions exchange when the material is immersed in body fluids. To investigate the Si^{4+} ions release from ceramics and the effect of porosity degree on the process, ICP-OES was used for a period of 6 weeks calculated in 10 time-points (0, 6, 12, 24 hours, 2, 4, 8 days, 2, 4, 6 weeks) with the materials immersed in α-MEM.

Figure 21 shows the differential ion release of the tested materials synthesized with a Loctite® 5248™ concentration of 7% presenting a small porosity (SiON7%), 5% presenting a medium porosity (SiON5%), 3% presenting a large porosity (SiON3%) and 5% for the flat material (Flat SiON). As expected, the Flat SiON shows the lower ion release capacity if compared with the other materials, probably due to the lower surface area exposed to the medium action. The ion release kinetic presents a common trend for all the porous SiON within 4 days. After that period, the dynamic starts to differentiate with the large porosity sample having the higher release ability. Si^{4+} release increase with the pores diameter and decrease with the concentration increase. The values obtained after 6 weeks of medium immersion were 61,8 ± 0,8 ppm for SiON7%, 74,2 ± 0,8 ppm for SiON5%, 88,1 ± 0,3 ppm for SiON3% and 39,5 ± 0,5 ppm for the flat material (Fig. 21). Generally, a decrease in surface pores dimension, for a constant surface, leads to an increase in surface area and consequently to a higher material exposition to the external agents, in this case, the ions exchange. The release differences in our case are probably correlated with the different concentrations used for the synthesis of the samples.
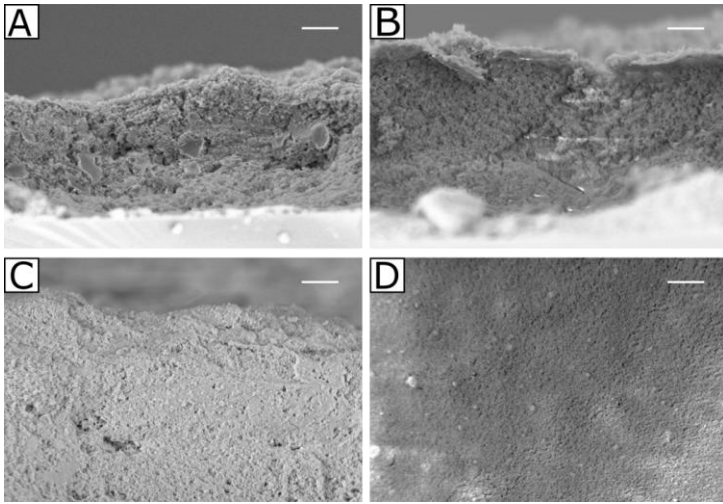
Figure 22 High resolution scanning electron microscopy of A) SiON7%, B) SiON5% and C) SiON3%. D) Flat surface view. Scale bar 2 µm.

Figure 22 shows the high resolution of the ceramics pores wall after break in liquid nitrogen (Fig.22 A, B and C) and the Flat SiON surface. It is clearly visible a difference in material consistency using different concentration for the pre-ceramic synthesis. SiON made with a lower alcoxysilane concentration (SiON3%, Fig.22 A) shows a low compactness surface with cavities and roughness in the nanometric dimensions. This effect is the result of the pyrolysis process in which all the organic carbon is combusted and removed from the material, creating voids and pores and increasing the exposed surface area. Increasing solutions concentration the effect is less visible (SiON5%, Fig.22 B) or not present (SiON7%, Fig.22 C), leading to the formation of a more compact and homogeneous structure with a decreased exposed surface area. This effect can explain the ICP-OES results correlating the surface area and the ion release. The flat sample (Fig.22 D) presents the lower release ability (Fig.21, black squares) due to the absence of the BF pattern and to the compact material structure. From these results, it is possible to assess that the precursor concentration, more than the surface pores dimension, affects the silicon ions release into the medium. These

phenomena could be also attributed to the surface free energy of the coatings which determines the wetting behavior in water environment. As explained before, the wettability of implantable materials determines protein kinetic adsorption from the body fluids, thus resulting important for guiding interactions with the host tissue and with cells.

To tests the samples wettability, sessile Contact Angle (CA) was measured. . The CA value for titanium alloy disks ($\theta = 67 \pm 2°$) was comparable with values reported in literature [159]. All the tested samples show a hydrophilic character, comparable with biomedical applications, in particular SiON7% $66 \pm 3°$, SiON5% $63 \pm 2°$ and SiON3% $66 \pm 2°$. Only for the Flat SiON samples the contract angle was significantly lower ($24 \pm 2°$) . The resultant wettability depends on the combination of chemical composition and surface nano and micro pattern. In this case the polar aminic groups of SiON and the surface pattern result in an hydrophilic CA. Comparing the results obtained for these materials with the data present in literature, the calculated CA combined with the specific chemical composition, are suitable for stem cells and osteoblasts adhesion [160,161].

3.4. SiON ceramic *in vitro* characterization

To assess the final osteoinductive potential of the surface porous SiON and the influence of porosity degree on ions release and cells response, the material was tested for Si^{4+} release, human Mesenchymal Stem Cells (hMSCs) adhesion, morphology, proliferation, metabolic and alkaline phosphatase activity modulation. As explained in previous paragraphs, chemical composition and surface topography are really important for cells responses when in contact with the material. The chemical composition can influence surface energy and molecule release, while the porous structure is involved in protein absorption and cell network formation. For these reasons three different porosity degrees were tested exploiting the capability of the BF process to tune the surface morphology. All the materials, in this case,

were synthesized coating Ti6Al4V disks and compared with the titanium alloy and with a flat SiON film, in order to assess the influence of porosity. The evaluation of potential osteoinductive effects was carried out on the samples with three different porosity degrees, using bone marrow derived human Mesenchymal Stem Cells (hMSCs). The effects of pores size and ions release on hMSCs were characterized in terms of adhesion, morphology, proliferation rate, metabolic activity and Alkaline Phosphatase (ALP) activity modulation.

3.4.1. Adhesion and morphology

Chemical composition and porosity degrees effects on hMSC adhesion, proliferation and morphology were evaluated through confocal microscopy at four different time-points: day 3, 7, 14 and 21 using, as control groups, tissue culture plates (TCP) and bare Ti6Al4V substrates (Fig23). As expected, control groups show a good initial adhesion, with a high proliferation rate over the time-points and a cells spindle-fibroblastic shape reaching a good confluence after 7 days (Fig.23 A1-4 and B1-4). On the flat coated metal samples (Flat SiON, Fig.23 C1-4) it is clearly visible a decrease in cells spreading and proliferation rate. Round shape hMSCs commonly indicates a tendency for adipose differentiation, but in this case, the low adhesion and proliferation can reasonably be attributed to an attempt of cells to reduce the area of contact with the material surface [162]. A clear example of this phenomenon is represented in figure 23 C-2 where cells tend to create a macroscopic aggregate instead of spreading on material surface. In comparison, on SiON3% and 7% (Fig.23 D1-4 and F1-4) a slight increase in initial adhesion and proliferation at different time-points are observable. Cells seeded on these two coatings present a mixed round and spindle-shape showing a higher proliferation rate after 14 and 21 days of incubation. Attempts of cells cytoskeleton to surround the pores edges, trying to establish a contact with those on the opposite side were observed in SiON3% samples (Fig.23 F4). hMSCs seeded on SiON5% have a

comparable behavior with those seeded on the control groups (Fig.23 E1-4). Cells show a good initial adhesion and proliferation rate with a spindle-fibroblastic shape and a good confluence after 7 days of incubation.
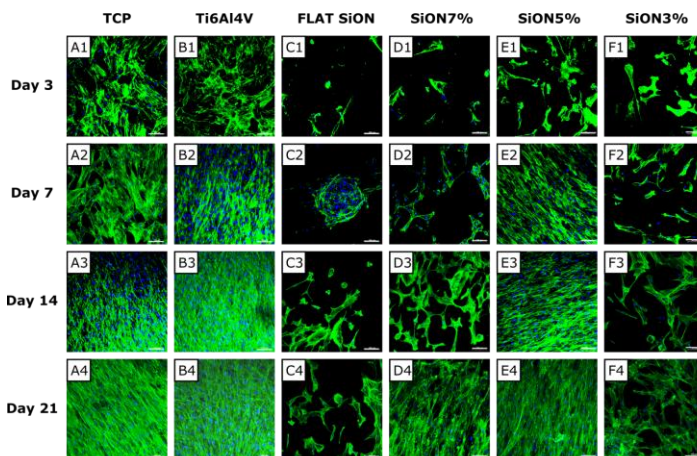
Figure 23 Confocal Images of hMSC seeded on TCP, Ti6Al4V, Flat SiON and the SiON made with concentrations of 7%, 5% and 3% after 3 (A1-F1), 7 (A2-F2), 14 A3-F3) and 21 (A4-F4) days of culture. Scale bar 100μm. Adapted from Carlomagno *et al* [163]

The reason for this behavior can be attributed to the morphology present on the coating, which induces a better cells adhesion and proliferation if compared with SiON 3% and 7%. hMSCs have the ability to proliferate creating a multi-layer structure, without presenting proliferation inhibition induced by contact. In this structure, all the cells are in contact with other cells through the network formed by the extracellular matrix (ECM), which also plays a fundamental role in cells spreading and adhesion driving the interactions of the cells with the surrounding environment. When the substrate is not optimal for cell interactions, an ECM layer is deposited on it allowing the adhesion and chemotaxis [164]. For this reason, substrates without suitable micrometric pattern for cells can cause a delay in adhesion and proliferation, also delaying the ECM production and secretion. An example of this phenomenon is given by the Flat SiON after 7 days of incubation

(Fig.23 C2). In this case, cells tend to create aggregates, rather than adhere on the coating. In these structures, cells present a round shape becoming quiescent under the proliferative point of view, but maintaining a high metabolic activity and proliferative potential [165,166]. At following time-points, cells restart spreading and proliferating, reasonably, after ECM deposition on the Flat SiON.

3.4.2. Proliferation rate, metabolic and ALP activity

Cells proliferation rate was quantitatively measured using the PicoGreen assay on all the produced samples at 4 different time-points (3, 7, 14 and 21 days, Fig.24 A). The reported data result in agreement with the qualitative analysis reported in the confocal microscopic images (Fig.23). Proliferation over the time-points and final cell number at day 21 are comparable on TCP, bare Ti6Al4V samples and SiON5% coated samples. The higher final cell number for TCP is probably due to the higher surface area available for their spreading and proliferation if compared with values obtained on the titanium disks (1,9 cm^2 for TCP and 1,5cm^2 for coated and uncoated Ti6Al4V disks). This observation was confirmed by the data normalized on the surface area value (data not shown). Other samples present a slower proliferation during the first three time-points, increasing after 21 days of culture (Fig.24 A Flat SiON, SiON3%, 5% and 7%). As explained before, this phenomenon can be induced by not the optimal micrometric structure, which, influencing cells-cells and cells-material interactions, can slow down the spreading process. After 21 days, cells number increase considerably, creating a multi-layered 3D structure. Proliferation rate data are a demonstration of the effects of substrate pattern on the cells processes. The Flat SiON presents a nanometric random porosity which, from the surface is recognized as nanometric sized roughness not in the correct range to induce favorable cells interactions. The main reason can be found in the protein absorption from the environment. The nanometric structure principally influences the absorption of protein on its surface inducing different substrate-adhesion protein interactions. This

characteristic highly affects the integrins expressed and recruited by the cells. This cascade affects in a significant way hMSCs adhesion, proliferation and differentiation toward a specific cell phenotype highlighting the close relationship between surface topography and cells fate [167,168]. An increase in pores dimension and substrate density (Fig.24 A, SiON7%), is able to induce a slight increase in cells spreading compared to the Flat sample, but the micrometric structure is still not optimal for the instauration of focal adhesions between cells and material surface [166,169]. There are different types of focal adhesions, varying from 1 to dozens of microns [170]. Surface micrometric topography can drive the formation or degradation of specific adhesions, as well as the nanometric structures influence integrins expression. As result, the formation of specific adhesions, in function of the surface pattern, can influence cells behavior and metabolism in terms of adhesion, spreading, movement and proliferation driving also the differentiation of stem cells [46]. A further increase in pores diameter up to 155 µm and 71 µm, with a decrease in substrate density, obstacle the cells-cells interactions avoiding cell contact, which is fundamental for proliferation and the creation of a network. In this case, hMSC start to secrete ECM, covering the surrounding surface, and then spreading on it to reach the cell-cell contact. For this reason, a delay in proliferation is observable up to 14 days. Ti6Al4V is a good material for bone tissue progenitor cells adhesion and proliferation due to the presence of a thin TiO_x layer on its surface [171]. This effect leads to a high proliferation rate during all the time-points and to a high final cell number (Fig.24 A, Ti6Al4V). The high proliferation induced by the Ti alloy is an expected result and for this reason was used as control for the evaluation of the other samples. Among the SiON samples tested, SiON5% presents the most suitable effect on seeded hMSCs (Fig.24 A, SiON5%). The micro- and nanostructure combination induce an optimal initial adhesion by cells and a fast proliferation comparable with the one of the control group. Even at day 21 the final cells number is optimal if compared with both the control groups and the other SiON coatings. The combination of nanostructure and

76

microstructure (pores diameter of 34 µm and 58 µm) are suitable for good cells adhesion and fast growth probably due to the similarity with bone marrow structure [172]. Cells metabolic activity shows an inverse trend respect to the PicoGreen (Fig.24 B). The metabolic activity is high where the proliferation rate is slow and vice versa. The materials with the lower proliferation, Flat SiON, SiON7% and 3%, show an increase in metabolic activity in the first two time-points (3 and 7 days) with a decrease for the last two (14 and 21 days) when the proliferation starts to increase (Fig.24 A and B, Flat SiON, SiON7% and SiON3%). The reason for this trend can be attributed to the necessity of production and secretion of a large amount of ECM for cells spreading. ECM makes the substrate more suitable for cells growth and its production necessitate an increase in metabolic activity [173]. Materials with a good proliferation, (Fig.24 A TCP, Ti6Al4V and SiON5%) show a lower metabolic activity during all the time-points (Fig. 24 B TCP, Ti6Al4V and SiON5%) reasonably because of the lower necessity of ECM production and secretion. ALP activity is reported in figure 24 C for TCP, Ti6Al4V, Flat SiON, SiON3%, 5% and 7% after 3, 7, 14 and 21 days. The effects of silicon ions on stem cells and cells related with the bone tissue has been already studied both *in vivo* and *in vitro* showing a direct relationship between ions concentration and ALP activity [25,35,42,174,175]. Our study confirms the close relationship between the two activities, with a higher ALP modulation for materials able to release a higher quantity of silicon ions (Fig.24 C, Flat SiON, SiON3%, 5% and 7%). TCP and Titanium alloy show only a slight increase in ALP activity during the experimental time-points (Fig.24 C).
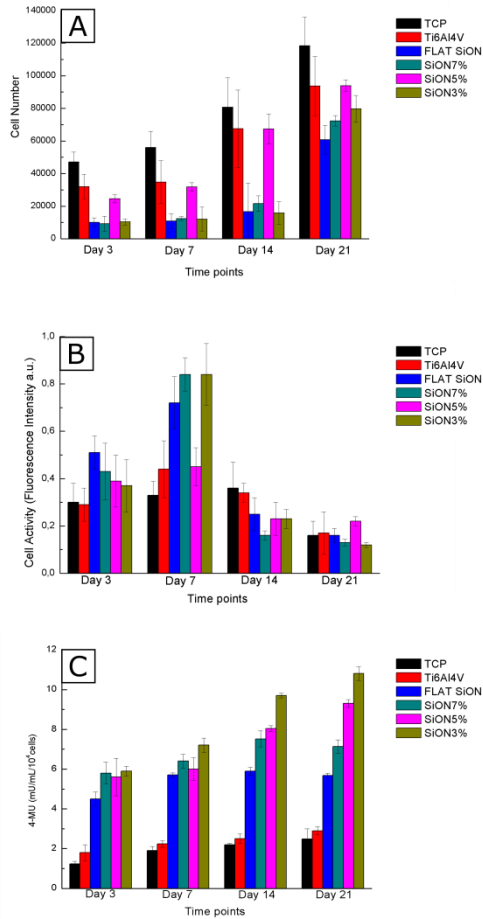
Figure 24 hMSCs A) proliferation rate quantified by PicoGreen, B) metabolic activity by AlamarBlue® and C) ALP activity modulation induced in cells seeded on TCP, Titanium-6-Aluminum-4-Vanadium (Ti6Al4V), silicon oxycarbide coatings made with a Loctite® 5248™ concentration of 7% (SiON7%, large porosity), 5% (SiON5%, medium porosity) and 7% (SiON7%, small porosity). Adapted from Carlomagno *et al*[163]

Flat SiON is the material with the lower released quantity (Fig.21) among the tested ceramics and shows a moderate increment in the first two time-points, while, a plateau phase is reached in the last two (Fig.24 C, Flat

SiON). The three materials with the highest release value (Fig.21 SiON3%, 5% and 7%), demonstrated also the highest enzyme activity modulation for all the tested time-points, confirming the correlation between ALP and silicon ions. The ALP enzyme is involved in many important functions, not only in the bone tissue. An increase in the enzyme activity is usually associated with osteogenic differentiation, maturation of bone tissue-forming cells, mineralization of collagen type I network and during the synthesis and secretion of ECM [174]. This marker is usually used as indicator of the material suitability for bone contact applications, demonstrating the potential use of the SiON materials in the biomedical field.

4.   Conclusions

Implant coatings are a class of materials with the role to act as a "bridge" between the metal prosthesis and the biological environment inducing rapid bone formation and strong metal-bone bonding. This role is achieved through the two main properties of the material: chemical composition and surface pattern. Many materials have been proposed for this application, including metals, polymers and ceramics. Among them, few materials possess the optimal mechanical strength and the ability to form a strong metal bone bonding. Moreover, the osteoinductive effect is present only in two of them: hydroxyapatite and Bioglasses®, which present limitations in the synthesis process in terms of metal bonding strength and resultant specific surface pattern. For these reason, an optimal material, which presents all the necessary properties to be used as implant coating with also a simple and high controllable process for its synthesis, is still under study. In last few years a new class of ceramics, called silicon oxynitrides, has been proposed for this application. Silicon oxynitride is a ceramic with optimal mechanical properties and high thermal, chemical and physical resistance. When synthesized at specific conditions, a strong titanium-ceramic ionic bond is formed, ensuring a strong metal adhesion and avoiding delamination when implanted. *In vivo* and *in vitro* tests showed also a potential osteoinductive effect when in contact whit the bone tissue. Nowadays, this

material is synthesized using very expensive and time-consuming techniques, with a low or null control on surface pattern and coating thickness, limiting the application and delaying the research progress. In this work we demonstrated a new route to obtain surface porous silicon-based ceramics, including silicon oxynitride, with a specific controllable pattern through. The BF process was performed using an UV-photo cross-linkable alkoxy silicone, already used in the biomedical field, called Loctite® 5248™. The high control on process variables allows to test their effect, individually or combined, on the final surface pattern. Pores diameter, density, distribution and order are strictly correlated with the time in which the solution is exposed to the humid environment and to the starting solution concentration. In particular, an increase in pre-exposure time leads to an increase in pores diameter and, at the same time, to the formation of a bimodal pores distribution. In the same way a decrease in solution concentration, decrease the system viscosity allowing the formation of larger pores. The precursor concentration affects also the order of the pattern. Low concentrations lead to the formation of random disposition, while, a high solution concentration can induce the formation of the typical high-packed honeycomb pattern. We tested also the surfactant presence effects on the final BF for two main reasons: facilitate the BF formation and functionalize the pores surface with a specific functional group. As expected, the addition of amphiphilic molecules facilitates the drops penetration due to the decrease in water/solution surface tension. Pores shape and dimension can be also modified by performing another technique in BF regime. The spin-coating allows flat solution surfaces removing the concentration gradient given by the normal casting process. Combining spin-coating and BF process, a ordered high-packed honeycomb patter was obtained. To be used as implant coatings, these materials must be applied on 3D metal surfaces with different shapes and we were able to coat different shaped objects performing the BF process using as substrate a water surface. This technique allows to coat also materials with a complex structure, such as titanium screws used for dental implants. After the BF process characterization, all

the materials underwent through heat treatments in order to evaluate the structure preservation and ceramic conversion. The ceramic final chemical composition is dependent on the used environment during the treatment, in particular using a inert gas such as nitrogen, a reorganization in the Si-O-C network was induced obtaining a silicon oxycarbide glass. Oxidant flowing gasses induce the complete removal of the organic carbon present in the material through combustion. In air atmosphere, the pre-ceramic was converted into silicon dioxide, while, under flowing ammonia, also nitridation occurs leading to the formation of a silicon oxynitride ceramic. The potential osteoinductivity of the SiON glasses was tested, first of all, through the quantification of silicon ion release in a physiological-like medium revealing a concentration dependent release dynamic. In particular, the behaviour which most affects the release in BF samples, is the concentration used for the synthesis more than the pores diameter and distribution. *In vitro* biological evaluations were carried out testing bone marrow derived human Mesenchymal Stem Cells adhesion, morphology, proliferation rate, metabolic and alkaline phosphatase activity. Confocal images show different adhesion, morphology and proliferation of hMSC depending on the substrate geometry. The most suitable material was the one made with a concentration of Loctite® 5248™ of 5% with a mean pores diameter of 34.3 ± 0.2 µm and 58.8 ± 0.6 µm, while, the other SiON coatings show a delay in proliferation and a lower initial adhesion. The quantitative analysis of the cell DNA content confirmed the results obtained from the confocal images. SiON5% shows a proliferation rate and final cell number comparable with the one of cells seeded on Ti6Al4V, where the other SiON ceramics show a delay in proliferation and lower initial adhesion. Cells metabolic activity shows a close relationship with the proliferative condition at each experimental time-point. When cells encounter difficulties in adhesion and proliferation, a higher metabolic activity was observed (Flat SiON, SiON3% and 7%), vice versa, highly proliferative cells demonstrated a lower metabolic activity (SiON5% and Ti6Al4V). During the proliferation state, all the materials show a decrease in

metabolic activity indicating a lower energy required for proliferation. The alkaline phosphatase activity is used as marker associated with osteogenic differentiation, maturation of bone tissue-forming cells, mineralization of collagen type I network and during the synthesis and secretion of ECM. It has been demonstrated that this enzyme is strictly correlated with the environmental silicon ions concentration and these phenomena was confirmed by our results. All the SiON coatings able to release silicon ions were able to positively modulate the ALP activity respect to the control group (TCP and Ti6Al4V). Surface topography, together with chemical composition, is a material characteristic able to drive cells phenomena such as adhesion, morphology, proliferation, activity, ECM secretion, protein expression and differentiation. A fundamental aspect of the used synthesis technique is the fine control on the final surface topography of the material. Despite many studies, the optimal surface pattern to enhance cells response is still under studies. All the cell phenotypes have one or more, single or combined ideal topographies in which can adhere, proliferate and eventually differentiate and produce specific extracellular matrix without the need of external stimuli. Our study demonstrated that silicon oxynitride, synthesized through the BF process, possess the potential to be used as implant coating in bone healing purposes. Despite different studies have been done on the bioactivity of SiON, there is a lack of results regarding the effect of this material with different surface pattern *in vivo*. As explained before, the surface pattern can play a role at the nano, micro and macro level and also different combination of porosities are able to induce multiple effects on different cell phenotypes. The exploration of these effects *in vivo* could be the definitive proof of the bioactivity of surface patterned SiON defining a specific pores range at the physiological level that can be also translated for other material for both *in vivo* and *in vitro* applications. Our work define an optimal pores range in order to induce fast cells adhesion and proliferation comparable with the one induced by titanium alloys. This response is probably a combination of suitable pores geometry and optimal silicon ions release. The role of the different porosities (nanoroughness, different

microporosity) on material surface must be deeply considered trying to test different pattern. Other effects can be evaluated both *in vitro* and *in vivo* modifying other process parameters. For example the material surface can be functionalized combining the ceramic with the biological coating (e.g. RGD, HAP nanoparticles, BMP-2) evaluating the cells and tissues response. Also other parameters such as the crystallinity obtained during the pyrolysis step or the ratio between SiO and Si_3N_4 and SiON can be biologically evaluated having a potential effect on cells differentiation and consecutive bone formation. The same route can be followed for the other two silicon-based ceramics synthesized confirming the many studies present in literature about the hemocompatibility of silicon oxycarbide and about the inert activity of silicon dioxide when applied as middle-ear coating. The transversal importance of the study rely on the application of the described BF process to create different Si-based ceramics applicable in specific fields with a process which represent a high save of time and costs and at the same time, showing the potential to be easily performed at the industrial level. One important advantage is represented by the strong ionic bond between -Ti-O-Si- formed during the heat treatments for the ceramic conversion. As explained in previous chapter, one of the main problem of the implant coatings is the delamination and possible formation of debris, which can induce the formation of a fibrotic capsule and consequent implant failure. The strong ionic bond combined with the potential osteoinductive surface represent a promising route to avoid prosthesis failure.

The importance of porous silicon based materials has been demonstrated in different fields of application where, nowadays, highly time-consuming, expensive and complicated techniques are used with, in some case, a limited control on the final result. In this study we presented a new technique able to produce silicon-based ceramic films with different chemical composition and specific surface porosity. All the synthesized materials can be used in different field of application without the necessity to combine different techniques (e.g. synthesis and lithography) and starting from the same

precursor. The BF method represent a easy, fast and cheap technique that can be applied on large scale, with a high repeatability and with different precursor.

Bibliography

1.   Parcianello G, Bernardo E, Colombo P, et al. Preceramic Polymer-Derived SiAlON as Sintering Aid for Silicon Nitride. Soraru G, ed. *J Am Ceram Soc*. 2014;97(11):3407-3412. doi:10.1111/jace.13134

2.   Colombo P, Mera G, Riedel R, Sorarù GD. Polymer-Derived Ceramics: 40 Years of Research and Innovation in Advanced Ceramics. *J Am Ceram Soc*. 2010;93(7):no-no. doi:10.1111/j.1551-2916.2010.03876.x

3.   Sarkar S, Chunder A, Fei W, An L, Zhai L. Superhydrophobic Mats of Polymer-Derived Ceramic Fibers. *J Am Ceram Soc*. 2008;91(8):2751-2755. doi:10.1111/j.1551-2916.2008.02500.x

4.   Pauthe M, Phalippou J, Belot V, Corriu R, Leclercq D, Vioux A. Preparation of oxynitride silicon glass I. Nitridation of hydrogenosilsesquioxane xerogels. *J Non Cryst Solids*. 1990;125(3):187-194. doi:10.1016/0022-3093(90)90848-G

5.   RIEDEL R, MERA G, HAUSER R, KLONCZYNSKI A. Silicon-Based Polymer-Derived Ceramics: Synthesis Properties and Applications-A Review. *J Ceram Soc Japan*. 2006;114(1330):425-444. doi:10.2109/jcersj.114.425

6.   Hu T, Li X, Pu W, Chu Z, Li G, Wang Q. Models Proposed to Explain the Electrical Conductivity of Polymer-Derived Silicon Carbide Fibers. Kleebe H-J, ed. *J Am Ceram Soc*. 2017;100(1):167-175. doi:10.1111/jace.14479

7.   Bacque E, Pillot JP, Birot M, Dunogues J. New polycarbosilane models. 1. Poly[(methylchlorosilylene)methylene], a novel, functional polycarbosilane. *Macromolecules*. 1988;21(1):30-34. doi:10.1021/ma00179a007

8.   de Wit P, Kappert EJ, Lohaus T, Wessling M, Nijmeijer A, Benes NE. Highly permeable and mechanically robust silicon carbide hollow fiber membranes. *J Memb Sci*. 2015;475:480-487. doi:10.1016/J.MEMSCI.2014.10.045

9.   Mera G, Riedel R, Poli F, Müller K. Carbon-rich SiCN ceramics derived from phenyl-containing poly(silylcarbodiimides). *J Eur Ceram Soc*. 2009;29(13):2873-2883. doi:10.1016/J.JEURCERAMSOC.2009.03.026

10.   Rahimi A, Shokrolahi P. Application of inorganic polymeric materials: I. Polysiloxanes. *Int J Inorg Mater*. 2001;3(7):843-847. doi:10.1016/S1466-6049(01)00162-3

11.   Finkelmann H, Kock H-J, Rehage G. Investigations on liquid crystalline polysiloxanes 3. Liquid crystalline elastomers — a new type of liquid crystalline material. *Die Makromol Chemie, Rapid Commun*. 1981;2(4):317-322. doi:10.1002/marc.1981.030020413

12.   Belot V, Corriu RJP, Leclercq D, Mutin PH, Vioux A. Thermal redistribution reactions in crosslinked polysiloxanes. *J Polym Sci Part A Polym Chem*. 1992;30(4):613-623. doi:10.1002/pola.1992.080300413

13.   Belot V, Corriu RJP, Leclercq D, Mutin PH, Vioux A. Thermal reactions occurring during pyrolysis of crosslinked polysiloxane gels, precursors to silicon oxycarbide glasses. *J Non Cryst Solids*. 1992;147-148:52-55. doi:10.1016/S0022-3093(05)80592-7

14.   Adam M, Vakifahmetoglu C, Colombo P, Wilhelm M, Grathwohl G. Polysiloxane-Derived Ceramics Containing Nanowires with Catalytically Active Tips. Soraru G, ed. *J Am Ceram Soc*. 2014;97(3):959-966. doi:10.1111/jace.12708

15.   Riedel R, Passing G, Schönfelder H, Brook RJ. Synthesis of dense silicon-based ceramics at low temperatures. *Nature*. 1992;355(6362):714-717. doi:10.1038/355714a0

16.   Studart AR, Gonzenbach UT, Tervoort E, Gauckler LJ. Processing Routes to Macroporous Ceramics: A Review. *J Am Ceram Soc*. 2006;89(6):1771-1789. doi:10.1111/j.1551-2916.2006.01044.x

17.   Biasetto L, Francis A, Palade P, Principi G, Colombo P. Polymer-derived microcellular SiOC foams with magnetic functionality. *J Mater Sci*. 2008;43(12):4119-4126. doi:10.1007/s10853-007-2224-3

18.   Bisi O, Ossicini S, Pavesi L. Porous silicon: a quantum sponge structure for silicon based optoelectronics. *Surf Sci Rep*. 2000;38(1-3):1-126. doi:10.1016/S0167-5729(99)00012-6

19.   Xu Y-N, Ching WY. Electronic structure and optical properties of α and β phases of silicon nitride, silicon oxynitride, and with comparison to silicon dioxide. *Phys Rev B*. 1995;51(24):17379-17389. doi:10.1103/PhysRevB.51.17379

20.   Sorarù GD, Modena S, Guadagnino E, Colombo P, Egan J, Pantano C. Chemical Durability of Silicon Oxycarbide Glasses. *J Am Ceram Soc*. 2002;85(6):1529-1536. doi:10.1111/j.1151-2916.2002.tb00308.x

21.   Bharadwaj L, Fan Y, Zhang L, Jiang D, An L. Oxidation Behavior of a Fully Dense Polymer-Derived Amorphous Silicon Carbonitride

Ceramic. *J Am Ceram Soc*. 2004;87(3):483-486. doi:10.1111/j.1551-2916.2004.00483.x

22.   Raj R, An L, Shah S, Riedel R, Fasel C, Kleebe H-J. Oxidation Kinetics of an Amorphous Silicon Carbonitride Ceramic. *J Am Ceram Soc*. 2004;84(8):1803-1810. doi:10.1111/j.1151-2916.2001.tb00918.x

23.   Mutin PH. Control of the composition and structure of silicon oxycarbide and oxynitride glasses derived from polysiloxane precursors. *J Sol-Gel Sci Technol*. 1999;14(1):27-38. doi:10.1023/A:1008769913083

24.   Hammel EC, Ighodaro O.-ROL-R, Okoli OI. Processing and properties of advanced porous ceramics: An application based review. *Ceram Int*. 2014;40(10):15351-15370. doi:10.1016/j.ceramint.2014.06.095

25.   Ilyas A, Lavrik N V., Kim HKW, Aswath PB, Varanasi VG. Enhanced Interfacial Adhesion and Osteogenesis for Rapid "bone-like" Biomineralization by PECVD-Based Silicon Oxynitride Overlays. *ACS Appl Mater Interfaces*. 2015;7(28):15368-15379. doi:10.1021/acsami.5b03319

26.   RIEDEL R, MERA G, HAUSER R, KLONCZYNSKI A. Silicon-Based Polymer-Derived Ceramics: Synthesis Properties and Applications-A Review. *J Ceram Soc Japan*. 2006;114(1330):425-444. doi:10.2109/jcersj.114.425

27.   Lu Z, Liu N, Lee H-W, et al. Nonfilling Carbon Coating of Porous Silicon Micrometer-Sized Particles for High-Performance Lithium Battery Anodes. *ACS Nano*. 2015;9(3):2540-2547. doi:10.1021/nn505410q

28.   Ozdemir S, Gole JL. The potential of porous silicon gas sensors. *Curr Opin Solid State Mater Sci*. 2007;11(5-6):92-100. doi:10.1016/J.COSSMS.2008.06.003

29.   Pickering C, Beale MIJ, Robbins DJ, Pearson PJ, Greef R. Optical studies of the structure of porous silicon films formed in p-type degenerate and non-degenerate silicon. *J Phys C Solid State Phys*. 1984;17(35):6535-6552. doi:10.1088/0022-3719/17/35/020

30.   Prasad A, Balakrishnan S, Jain SK, Jain GC. Porous Silicon Oxide Anti-Reflection Coating for Solar Cells. http://jes.ecsdl.org/content/129/3/596.full.pdf. Accessed April 10, 2017.

31.   Ehlert N, Mueller PP, Stieve M, Lenarz T, Behrens P. Mesoporous silica films as a novel biomaterial: applications in the middle ear. *Chem Soc Rev*. 2013;42(9):3847. doi:10.1039/c3cs35359a

32.   Zhuo R, Colombo P, Pantano C, Vogler E a. Silicon oxycarbide glasses for blood-contact applications. *Acta Biomater*. 2005;1(5):583-589. doi:10.1016/j.actbio.2005.05.005

33.   Renlund GM, Prochazka S, Doremus RH. Silicon oxycarbide glasses: Part II. Structure and properties. *J Mater Res*. 1991;6(12):2723-2734. doi:10.1557/JMR.1991.2723

34.   Peters D, Fischer K, Müller J. Integrated optics based on silicon oxynitride thin films deposited on silicon substrates for sensor applications. *Sensors Actuators A Phys*. 1991;26(1-3):425-431. doi:10.1016/0924-4247(91)87026-Y

35.   Ilyas A, Odatsu T, Shah A, et al. Amorphous Silica: A New Antioxidant Role for Rapid Critical-Sized Bone Defect Healing. *Adv Healthc Mater*. 2016;5(17):2199-2213.

doi:10.1002/adhm.201600203

36.   Liu Y, Lin I-K, Zhang X. Mechanical properties of sputtered silicon oxynitride films by nanoindentation. *Mater Sci Eng A*. 2008;489(1-2):294-301. doi:10.1016/j.msea.2008.01.063

37.   Lai W, Garino J, Ducheyne P. Silicon excretion from bioactive glass implanted in rabbit bone. *Biomaterials*. 2002;23(1):213-217. http://www.ncbi.nlm.nih.gov/pubmed/11762840.   Accessed February 5, 2018.

38.   Beletskii BI, Sventskaya N V. SILICON IN LIVING ORGANISMS AND NEW-GENERATION BIOCOMPOSITE MATERIALS (REVIEW). *Steklo i Keramika*. 2009;(3):26-30. https://link.springer.com/content/pdf/10.1007%2Fs10717-009-9136-4.pdf. Accessed February 5, 2018.

39.   Hench LL. Bioceramics. *J Am Ceram Soc*. 1998;28:1705-1728. doi:10.1111/j.1151-2916.1998.tb02540.x

40.   Knabe C, Berger G, Gildenhaar R, Howlett CR, Markovic B, Zreiqat H. The functional expression of human bone-derived cells grown on rapidly resorbable calcium phosphate ceramics. *Biomaterials*.   2004;25(2):335-344. http://www.ncbi.nlm.nih.gov/pubmed/14585721.   Accessed February 5, 2018.

41.   Xynos ID, Edgar AJ, Buttery LD, Hench LL, Polak JM. Gene-expression profiling of human osteoblasts following treatment with the ionic products of Bioglass 45S5 dissolution. *J Biomed Mater Res*.   2001;55(2):151-157. http://www.ncbi.nlm.nih.gov/pubmed/11255166.   Accessed February 5, 2018.

42.   Saffarian Tousi N, Velten MF, Bishop TJ, et al. Combinatorial effect of Si4 +, Ca2 +, and Mg 2 + released from bioactive glasses on osteoblast osteocalcin expression and biomineralization. *Mater Sci Eng C*. 2013;33(5):2757-2765. doi:10.1016/j.msec.2013.02.044

43.   Xynos ID, Hukkanen MVJ, Batten JJ, Buttery LD, Hench LL, Polak JM. Bioglass &sreg;45S5 Stimulates Osteoblast Turnover and Enhances Bone Formation In Vitro: Implications and Applications for Bone Tissue Engineering. 2000. doi:10.1007/s002230001134

44.   Gittens RA, Olivares-Navarrete R, Schwartz Z, Boyan BD. Implant osseointegration and the role of microroughness and nanostructures: Lessons for spine implants. *Acta Biomater*. 2014;10(8):3363-3371. doi:10.1016/j.actbio.2014.03.037

45.   CAVALCANTIADAM E, MICOULET A, BLUMMEL J, AUERNHEIMER J, KESSLER H, SPATZ J. Lateral spacing of integrin ligands influences cell spreading and focal adhesion assembly. *Eur J Cell Biol*. 2006;85(3-4):219-224. doi:10.1016/j.ejcb.2005.09.011

46.   Anselme K, Davidson P, Popa AM, Giazzon M, Liley M, Ploux L. The interaction of cells and bacteria with surfaces structured at the nanometre scale. *Acta Biomater*. 2010;6:3824-3846. doi:10.1016/j.actbio.2010.04.001

47.   Forgacs G. On the possible role of cytoskeletal filamentous networks in intracellular signaling: an approach based on percolation. *J Cell Sci*. 1995;108 (Pt 6):2131-2143. http://www.ncbi.nlm.nih.gov/pubmed/7673334. Accessed January 25, 2018.

48.   Ingber DE. TENSEGRITY: THE ARCHITECTURAL BASIS OF

CELLULAR MECHANOTRANSDUCTION. *Annu Rev Physiol*.
1997;59(1):575-599. doi:10.1146/annurev.physiol.59.1.575

49.   Tranquillo RT. Self-organization of tissue-equivalents: the nature
        and role of contact guidance. *Biochem Soc Symp*. 1999;65:27-42.
        http://www.ncbi.nlm.nih.gov/pubmed/10320931. Accessed January
        26, 2018.

50.   Eisenbarth E, Linez P, Biehl V, Velten D, Breme J, Hildebrand H.
        Cell orientation and cytoskeleton organisation on ground titanium
        surfaces. *Biomol Eng*. 2002;19(2-6):233-237. doi:10.1016/S1389-
        0344(02)00028-X

51.   Baksh D, Davies JE, Kim S. Three-dimensional matrices of calcium
        polyphosphates support bone growth in vitro and in vivo. *J Mater
        Sci   Mater   Med*.   1998;9(12):743-748.
        doi:10.1023/A:1008959103864

52.   Lee SJ, Lee IW, Lee YM, Lee HB, Khang G. Macroporous
        biodegradable natural/synthetic hybrid scaffolds as small intestine
        submucosa impregnated poly(D,L-lactide-co-glycolide) for tissue-
        engineered bone. *J Biomater Sci Polym Ed*. 2004;15(8):1003-1017.
        http://www.ncbi.nlm.nih.gov/pubmed/15461186. Accessed January
        25, 2018.

53.   Nehrer S, Breinan HA, Ramappa A, et al. Matrix collagen type and
        pore size influence behaviour of seeded canine chondrocytes.
        Biomaterials.   1997;18(11):769-776.
        http://www.ncbi.nlm.nih.gov/pubmed/9177854. Accessed January
        25, 2018.

54.   Pilliar RM, Lee JM, Maniatopoulos C. Observations on the Effect
        of Movement on Bone Ingrowth into Porous-Surfaced Implants.
        Clin   Orthop   Relat   Res.   1986;208(208):108-113.

doi:10.1097/00003086-198607000-00023

55.   Williams JM, Adewunmi A, Schek RM, et al. Bone tissue engineering using polycaprolactone scaffolds fabricated via selective laser sintering. *Biomaterials*. 2005;26(23):4817-4827. doi:10.1016/j.biomaterials.2004.11.057

56.   Puleo DA, Nanci A. Understanding and controlling the bone}implant interface. *Biomaterials*. 1999;20:2311-2321. https://ac.els-cdn.com/S014296129900160X/1-s2.0-S014296129900160X-main.pdf?_tid=fd2074b6-01b7-11e8-bd43-00000aab0f01&acdnat=1516875217_52b0ed4576419adee5418fe7f18977bb. Accessed January 25, 2018.

57.   Brunette DM, Chehroudi B. The Effects of the Surface Topography of Micromachined Titanium Substrata on Cell Behavior in Vitro and in Vivo. *J Biomech Eng*. 1999;121(1):49. doi:10.1115/1.2798042

58.   Correa VL, Garza KM, Murr LE. Vascularization in interconnected 3D printed Ti-6Al-4V foams with hydrogel matrix for biomedical bone replacement implants. *Sci China Mater*. October 2017:1-14. doi:10.1007/s40843-017-9091-1

59.   Vandrovcova M, Hanus J, Drabik M, et al. Effect of different surface nanoroughness of titanium dioxide films on the growth of human osteoblast-like MG63 cells. *J Biomed Mater Res Part A*. 2012;100A(4):1016-1032. doi:10.1002/jbm.a.34047

60.   Padial-Molina M, Galindo-Moreno P, Fernández-Barbero JE, et al. Role of wettability and nanoroughness on interactions between osteoblast and modified silicon surfaces. *Acta Biomater*. 2011;7(2):771-778. doi:10.1016/J.ACTBIO.2010.08.024

61.   Kuroda D, Niinomi M, Morinaga M, Kato Y, Yashiro T. Design
        and mechanical properties of new β type titanium alloys for implant
        materials. *Mater   Sci   Eng   A*.   1998;243(1-2):244-249.
        doi:10.1016/S0921-5093(97)00808-3

62.   Liu X, Chu PK, Ding C. Surface modification of titanium, titanium
        alloys, and related materials for biomedical applications. *Mater Sci
        Eng   R   Reports*.   47(3-4):49-121.
        https://www.sciencedirect.com/science/article/pii/S0927796X04001
        24X. Accessed August 1, 2017.

63.   Sáenz De Viteri V, Fuentes E. Titanium and Titanium Alloys as
        Biomaterials. doi:10.5772/55860

64.   Materials MS. A quantitative comparison of the cell response to
        commercially pure titanium and Ti-6AI-4V implants in the
        abdominal   wall   of   rats.   1992;3(126).
        https://link.springer.com/content/pdf/10.1007%2FBF00705280.pdf.
        Accessed February 1, 2018.

65.   Van Noort R. Titanium: The implant material of today. *J Mater Sci*.
        1987;22(11):3801-3811. doi:10.1007/BF01133326

66.   Suska F, Emanuelsson L, Johansson A, Tengvall P, Thomsen P.
        Fibrous capsule formation around titanium and copper. *J Biomed
        Mater Res Part A*. 2008;85A(4):888-896. doi:10.1002/jbm.a.31575

67.   T. A, C. J. Osteoinduction, osteoconduction and osseointegration.
        Eur Spine J. 2001;10(0):S96-S101. doi:10.1007/s005860100282

68.   Hallab NJ, Jacobs JJ. Biologic effects of implant debris. *Bull NYU
        Hosp   Jt   Dis*.   2009;67(2):182-188.
        http://www.ncbi.nlm.nih.gov/pubmed/19583551.   Accessed
        February 1, 2018.

69.   E. H. Jeffery, K. Abreo, E. Burgess KAEBJCJLG. SYSTEMIC ALUMINUM TOXICITY: EFFECTS ON BONE, HEMATOPOIETIC TISSUE, AND KIDNEY. *J Toxicol Environ Health*. 1996;48(6):649-666. doi:10.1080/009841096161122

70.   YUMOTO S, OHASHI H, NAGAI H, et al. ALUMINUM NEUROTOXICITY IN THE RAT BRAIN. *Int J PIXE*. 1992;02(04):493-504. doi:10.1142/S0129083592000531

71.   Alfrey AC. Aluminum Toxicity in Humans. In: *Trace Elements in Clinical Medicine*. Tokyo: Springer Japan; 1990:459-464. doi:10.1007/978-4-431-68120-5_59

72.   Matsuno H, Yokoyama A, Watari F, Uo M, Kawasaki T. Biocompatibility and osteogenesis of refractory metal implants, titanium, hafnium, niobium, tantalum and rhenium. *Biomaterials*. 2001;22(11):1253-1262. http://www.ncbi.nlm.nih.gov/pubmed/11336297. Accessed February 1, 2018.

73.   Domingo JL. Vanadium: A review of the reproductive and developmental toxicity. *Reprod Toxicol*. 1996;10(3):175-182. doi:10.1016/0890-6238(96)00019-6

74.   Hanawa T. In vivo metallic biomaterials and surface modification. *Mater Sci Eng A*. 1999;267(2):260-266. doi:10.1016/S0921-5093(99)00101-X

75.   Geetha M, Singh AKK, Asokamani R, Gogia AKK. Ti based biomaterials, the ultimate choice for orthopaedic implants – A review. *Prog Mater Sci*. 2009;54(3):397-425. doi:10.1016/j.pmatsci.2008.06.004

76.   Xuereb M, Camilleri J, Attard NJ. Systematic Review of Current

Dental Implant Coating Materials and Novel Coating Techniques. *Int J Prosthodont*. 2015;2828(10). doi:10.11607/ijp.4124

77.   Okada M, Neo Y, Kubomura K, - al, Chen S-C, Tamura H. Coating Films of Titanium Nitride Prepared by Ion and Vapor Deposition Method Formation of Carbon Nitride Films by Means of Ion Assisted Dynamic Mixing (IVD) Method Fuminori Fujimoto and Kiyoshi Ogata - Structural and Emission Characteristics of Iron-Oxide Whiskers on a Steel Plate Formation of Titanium Nitride/Titanium Silicide by High Pressure Nitridation in Titanium/Silicon. *Japanese J Appl Phys Mamoru Satou al Jpn J Appl Phys*. 1985;24. http://iopscience.iop.org/article/10.1143/JJAP.24.656/pdf. Accessed February 2, 2018.

78.   Dion I, Baquey C, Candelon B, Monties JR. Hemocompatibility of titanium nitride. *Int J Artif Organs*. 1992;15(10):617-621. http://www.ncbi.nlm.nih.gov/pubmed/1428211. Accessed February 2, 2018.

79.   Sovak G, Weiss SA, Weiss A, Gotman I. THE JOURNAL OF BONE AND JOINT SURGERY Osseointegration of Ti6Al4V alloy implants coated with titanium nitride by a new method. *J Bone Jt Surg [Br]*. 2000;82:290-296. http://bjj.boneandjoint.org.uk/content/jbjsbr/82-B/2/290.full.pdf. Accessed February 2, 2018.

80.   Intemann A, Koerner H, Koch F. Film Properties of CVD Titanium Nitride Deposited with Organometallic Precursors at Low Pressure Using Inert Gases, Ammonia, or Remote Activation. *J Electrochem Soc*. 1993;140(11):3215. doi:10.1149/1.2221013

81.   C.E. J, J.M. T, J.C. J, H.I.M. Walenkamp G, J. P. Modern

Orthopaedic Implant Coatings — Their Pro's, Con's and Evaluation Methods. In: *Modern Surface Engineering Treatments*. InTech; 2013. doi:10.5772/55976

82.   Kantlehner M, Schaffner P, Finsinger D, et al. Surface coating with cyclic RGD peptides stimulates osteoblast adhesion and proliferation as well as bone formation. *Chembiochem*. 2000;1(2):107-114.
http://www.ncbi.nlm.nih.gov/pubmed/11828404. Accessed February 1, 2018.

83.   Alt V, Bitschnau A, Böhner F, et al. Effects of gentamicin and gentamicin–RGD coatings on bone ingrowth and biocompatibility of cementless joint prostheses: An experimental study in rabbits. *Acta Biomater*. 2011;7(3):1274-1280. doi:10.1016/j.actbio.2010.11.012

84.   Ardjomandi N, Klein C, Kohler K, et al. Indirect coating of RGD peptides using a poly-L-lysine spacer enhances jaw periosteal cell adhesion, proliferation, and differentiation into osteogenic tissue. *J Biomed Mater Res Part A*. 2012;100A(8):2034-2044. doi:10.1002/jbm.a.34062

85.   Chen G, Deng C, Li Y-P. TGF-β and BMP signaling in osteoblast differentiation and bone formation. *Int J Biol Sci*. 2012;8(2):272-288. doi:10.7150/ijbs.2929

86.   Liu Y, Wu G, de Groot K. Biomimetic coatings for bone tissue engineering of critical-sized defects. *J R Soc Interface*. 2010;7(Suppl_5):S631-S647. doi:10.1098/rsif.2010.0115.focus

87.   Rawlings RD. Bioactive Glasses and Glass-Ceramics. *Chrcuf Mater*. 1993;14:155-179. http://cyber.sci-hub.tw/MTAuMTAxNi8wMjY3LTY2MDUoOTMpOTAwMzgtO

Q==/10.1016%400267-6605%2893%2990038-9.pdf.   Accessed
February 2, 2018.

88.   Cheng L, Ye F, Yang R, et al. Osteoinduction of hydroxyapatite/β-
        tricalcium phosphate bioceramics in mice with a fractured fibula.
        Acta   Biomater.   2010;6(4):1569-1574.
        doi:10.1016/J.ACTBIO.2009.10.050

89.   Tsuruga E, Takita H, Itoh H, Wakisaka Y, Kuboki Y. Pore size of
        porous hydroxyapatite as the cell-substratum controls BMP-induced
        osteogenesis.   *J   Biochem*.   1997;121(2):317-324.
        http://www.ncbi.nlm.nih.gov/pubmed/9089406. Accessed February
        2, 2018.

90.   Oshida Y, Hashem A, Nishihara T, Yapchulay M V. Fractal
        dimension analysis of mandibular bones: toward a morphological
        compatibility of implants. *Biomed Mater Eng*. 1994;4(5):397-407.
        http://www.ncbi.nlm.nih.gov/pubmed/8000293. Accessed February
        2, 2018.

91.   Lin L, Chow KL, Leng Y. Study of hydroxyapatite osteoinductivity
        with an osteogenic differentiation of mesenchymal stem cells. *J
        Biomed   Mater   Res   Part   A*.   2009;89A(2):326-335.
        doi:10.1002/jbm.a.31994

92.   Hägi TT, Enggist L, Michel D, Ferguson SJ, Liu Y, Hunziker EB.
        Mechanical insertion properties of calcium-phosphate implant
        coatings. *Clin Oral Implants Res*. 2010;21(11):1214-1222.
        doi:10.1111/j.1600-0501.2010.01916.x

93.   Iezzi G, Scarano A, Petrone G, Piattelli A. Two Human
        Hydroxyapatite-Coated Dental Implants Retrieved After a 14-Year
        Loading Period: A Histologic and Histomorphometric Case Report.
        J Periodontol. 2007;78(5):940-947. doi:10.1902/jop.2007.060271

94.   Woodard JR, Hilldore AJ, Lan SK, et al. The mechanical properties and osteoconductivity of hydroxyapatite bone scaffolds with multi-scale porosity. *Biomaterials*. 2007;28(1):45-54. doi:10.1016/J.BIOMATERIALS.2006.08.021

95.   Palmquist A, Omar OM, Esposito M, Lausmaa J, Thomsen P. Titanium oral implants: surface characteristics, interface biology and clinical outcome. *J R Soc Interface*. 2010;7(Suppl_5):S515-S527. doi:10.1098/rsif.2010.0118.focus

96.   Mano T, Ueyama Y, Ishikawa K, Matsumura T, Suzuki K. Initial tissue response to a titanium implant coated with apatite at room temperature using a blast coating method. *Biomaterials*. 2002;23(9):1931-1936. http://www.ncbi.nlm.nih.gov/pubmed/11996033. Accessed February 2, 2018.

97.   Sola a, Bellucci D, Cannillo V, Cattini a. Bioactive glass coatings: a review. *Surf Eng*. 2011;27(8):560-572. doi:10.1179/1743294410Y.0000000008

98.   Hench LL. The story of Bioglass®. *J Mater Sci Mater Med*. 2006;17(11):967-978. doi:10.1007/s10856-006-0432-z

99.   Ylänen HO. *Bioactive Glasses : Materials, Properties and Applications*. https://books.google.it/books?id=pSYUDgAAQBAJ&pg=PA106&lpg=PA106&dq=bioglass+pro+and+cons&source=bl&ots=UhYGZAj2HM&sig=jsTVJiWlKtZ3JekCJJKxTYWFM9g&hl=it&sa=X&ved=0ahUKEwiplKOn_o7ZAhVB66QKHQ1PBzAQ6AEIajAH#v=onepage&q=bioglass pro cons&f=false. Accessed February 5, 2018.

100.   Mack CA. *Fundamental Principles of Optical Lithography : The*

Science of Microfabrication. Wiley; 2007. https://www.wiley.com/en-us/Fundamental+Principles+of+Optical+Lithography%3A+The+Science+of+Microfabrication-p-9780470018934. Accessed February 7, 2018.

101. Hallgren C, Reimers H, Gold J, Wennerberg A. The importance of surface texture for bone integration of screw shaped implants: Anin vivo study of implants patterned by photolithography. *J Biomed Mater Res*. 2001;57(4):485-496. doi:10.1002/1097-4636(20011215)57:4<485::AID-JBM1194>3.0.CO;2-1

102. Paíka V, Pos\ E, Koerten HK. Some characteristics of hydroxylapatite powder particles after plasma spraying. *Biomaterials*. 1998;19:1763-1772. https://ac.els-cdn.com/S0142961298000878/1-s2.0-S0142961298000878-main.pdf?_tid=1531009e-0c11-11e8-94f8-00000aacb361&acdnat=1518012995_15f71b660087222ddf999967ece92deb. Accessed February 7, 2018.

103. Ellies LG, Nelson DGA, Featherstone JDB. Crystallographic changes in calcium phosphates during plasma-spraying. *Biomaterials*. 1992;13(5):313-316. doi:10.1016/0142-9612(92)90055-S

104. Larker HT. Hot Isostatic Pressing of Ceramics. In: *Progress in Nitrogen Ceramics*. Dordrecht: Springer Netherlands; 1983:717-724. doi:10.1007/978-94-009-6851-6_61

105. Khor KA, Yip CS, Cheang P. Post-spray hot isostatic pressing of plasma sprayed Ti□6Al□4V/hydroxyapatite composite coatings. *J Mater Process Technol*. 1997;71(2):280-287. doi:10.1016/S0924-0136(97)00086-1

106.   Liang H, Shi B, Fairchild A, Cale T. Applications of plasma coatings in artificial joints: an overview. *Vacuum*. 2004;73(3-4):317-326. doi:10.1016/J.VACUUM.2003.12.160

107.   Tao S, Heng J, Chuanxian D. Effect of vapor-flame treatment on plasma sprayed hydroxyapatite coatings. *J Biomed Mater Res*. 2000;52(3):572-575. http://www.ncbi.nlm.nih.gov/pubmed/11007627.   Accessed February 7, 2018.

108.   Sonawane R., Kale B., Dongare M. Preparation and photo-catalytic activity of Fe☐TiO2 thin films prepared by sol–gel dip coating. *Mater   Chem   Phys*.   2004;85(1):52-57. doi:10.1016/J.MATCHEMPHYS.2003.12.007

109.   Aegerter MA, Mennig M. *Sol-Gel Technologies for Glass Producers and Users*. Springer US; 2004.

110.   Koch CF, Johnson S, Kumar D, et al. Pulsed laser deposition of hydroxyapatite thin films. *Mater Sci Eng C*. 2007;27(3):484-494. doi:10.1016/J.MSEC.2006.05.025

111.   Wei M, Ruys AJ, Milthorpe BK, Sorrell CC, Evans JH. Electrophoretic Deposition of Hydroxyapatite Coatings on Metal Substrates: A Nanoparticulate Dual-Coating Approach. *J Sol-Gel Sci Technol*. 2001;21(1/2):39-48. doi:10.1023/A:1011201414651

112.   Ma J, Liang CH, Kong LB, Wang C. Colloidal characterization and electrophoretic deposition of hydroxyapatite on titanium substrate. *J   Mater   Sci   Mater   Med*.   2003;14(9):797-801. doi:10.1023/A:1025092506583

113.   Brinker CJ, Ashley CS, Cairncross RA, et al. Sol—gel derived ceramic films — fundamentals and applications. In: *Metallurgical*

and Ceramic Protective Coatings. Dordrecht: Springer Netherlands; 1996:112-151. doi:10.1007/978-94-009-1501-5_6

114.   Olding T, Sayer M, Barrow D. Ceramic sol–gel composite coatings for electrical insulation. *Thin Solid Films*. 2001;398-399:581-586. doi:10.1016/S0040-6090(01)01322-0

115.   Cui F., Luo Z. Biomaterials modification by ion-beam processing. *Surf Coatings Technol*. 1999;112(1-3):278-285. doi:10.1016/S0257-8972(98)00763-4

116.   Hamdi M, Ide-Ektessabi A. Preparation of hydroxyapatite layer by ion beam assisted simultaneous vapor deposition. *Surf Coatings Technol*. 2003;163-164:362-367. doi:10.1016/S0257-8972(02)00625-4

117.   Hoa MLK, Lu M, Zhang Y. Preparation of porous materials with ordered hole structure. *Adv Colloid Interface Sci*. 2006;121(1-3):9-23. doi:10.1016/J.CIS.2006.05.029

118.   Huie JC. Guided molecular self-assembly: a review of recent efforts. *Smart Mater Struct*. 2003;12(2):264-271. doi:10.1088/0964-1726/12/2/315

119.   Velev OD, Lenhoff AM. Colloidal crystals as templates for porous materials. *Curr Opin Colloid Interface Sci*. 2000;5. http://crystal.che.ncsu.edu/pdfs/CurrOpin_review.pdf. Accessed February 26, 2018.

120.   Vladisavljević GT, Duncanson WJ, Shum HC, Weitz DA. Emulsion Templating of Poly(lactic acid) Particles: Droplet Formation Behavior. *Langmuir*. 2012;28(36):12948-12954. doi:10.1021/la302092f

121.   van de Witte P, Dijkstra PJ, van den Berg JWA, Feijen J. Phase

separation processes in polymer solutions in relation to membrane formation. *J Memb Sci*. 1996;117(1-2):1-31. doi:10.1016/0376-7388(96)00088-9

122.   Fritter D, Knobler CM, Beysens DA. Experiments and simulation of the growth of droplets on a surface (breath figures). *Phys Rev A*. 1991;43(6):2858-2869. doi:10.1103/PhysRevA.43.2858

123.   Srinivasarao M, Collings D, Philips A, Patel S. Three-dimensionally ordered array of air bubbles in a polymer film. *Science*. 2001;292(5514):79-83. doi:10.1126/science.1057887

124.   Zhang A, Bai H, Li L. Breath Figure: A Nature-Inspired Preparation Method for Ordered Porous Films. *Chem Rev*. 2015;115(18):9801-9868. doi:10.1021/acs.chemrev.5b00069

125.   Widawski G, Rawiso M, François B. Self-organized honeycomb morphology of star-polymer polystyrene films. *Nature*. 1994;369(6479):387-389. doi:10.1038/369387a0

126.   Bai H, Du C, Zhang A, Li L. Breath figure arrays: Unconventional fabrications, functionalizations, and applications. *Angew Chemie - Int Ed*. 2013;52(47):12240-12255. doi:10.1002/anie.201303594

127.   Steyer, Guenoun, Beysens, Knobler. Two-dimensional ordering during droplet growth on a liquid surface. *Phys Rev B Condens Matter*. 1990;42(1):1086-1089. http://www.ncbi.nlm.nih.gov/pubmed/9994664. Accessed March 5, 2018.

128.   Wan L-S, Zhu L-W, Ou Y, Xu Z-K. Multiple interfaces in self-assembled breath figures. *Chem Commun*. 2014;50(31):4024-4039. doi:10.1039/c3cc49826c

129.   Steyer, Guenoun, Beysens. Hexatic and fat-fractal structures for

water droplets condensing on oil. *Phys Rev E Stat Phys Plasmas Fluids Relat Interdisc Topics*. 1993;48(1):428-431. http://www.ncbi.nlm.nih.gov/pubmed/9960604. Accessed March 5, 2018.

130.   Saunders AE, Dickson JL, Shah PS, et al. Breath figure templated self-assembly of porous diblock copolymer films. *Phys Rev E*. 2006;73(3):031608. doi:10.1103/PhysRevE.73.031608

131.   Servoli E, Ruffo G a., Migliaresi C. Interplay of kinetics and interfacial interactions in breath figure templating – A phenomenological interpretation. *Polymer (Guildf)*. 2010;51(11):2337-2344. doi:10.1016/j.polymer.2010.03.039

132.   Bergman TL, Incropera FP. *Fundamentals of Heat and Mass Transfer.* Wiley; 2011. https://books.google.it/books?hl=it&lr=&id=vvyIoXEywMoC&oi=fnd&pg=PR21&dq=mass+transfer+rayleigh+number&ots=8JpgMZiWF6&sig=lHsPVimPw8MAAUw9mcrw38gxEvM#v=onepage&q=mass transfer rayleigh number&f=false. Accessed March 6, 2018.

133.   Semwogerere D, Schatz MF. Evolution of Hexagonal Patterns from Controlled Initial Conditions in a Bénard-Marangoni Convection Experiment. *Phys Rev Lett*. 2002;88(5):054501. doi:10.1103/PhysRevLett.88.054501

134.   Ma M, Gupta M, Li Z, et al. Decorated Electrospun Fibers Exhibiting Superhydrophobicity. *Adv Mater*. 2007;19(2):255-259. doi:10.1002/adma.200601449

135.   Tian Y, Jiao Q, Ding H, Shi Y, Liu B. The formation of honeycomb structure in polyphenylene oxide films. *Polymer (Guildf)*. 2006;47(11):3866-3873. doi:10.1016/J.POLYMER.2006.03.081

136. Peng J, Han Y, Yang Y, Li B. The influencing factors on the macroporous formation in polymer films by water droplet templating. *Polymer (Guildf)*. 2004;45(2):447-452. https://www.sciencedirect.com/science/article/pii/S0032386103010760. Accessed August 8, 2017.

137. Bunz UHF. Breath figures as a dynamic templating method for polymers and nanomaterials. *Adv Mater*. 2006;18(8):973-989. doi:10.1002/adma.200501131

138. Jiang X, Zhou X, Zhang Y, Zhang T, Guo Z, Gu N. Interfacial Effects of *In Situ* -Synthesized Ag Nanoparticles on Breath Figures. *Langmuir*. 2010;26(4):2477-2483. doi:10.1021/la9027139

139. Sun H, Li H, Wu L. Micro-patterned polystyrene surfaces directed by surfactant-encapsulated polyoxometalate complex via breath figures. *Polymer (Guildf)*. 2009;50(9):2113-2122. doi:10.1016/J.POLYMER.2009.02.036

140. Englert BC, Scholz S, Leech PJ, Srinivasarao M, Bunz UHF. Templated ceramic microstructures by using the breath-figure method. *Chem - A Eur J*. 2005;11(3):995-1000. doi:10.1002/chem.200400921

141. Gong J, Xu B, Tao X, et al. Templated ceramic microstructures by using the breath-figure method. *Plasma Process Polym*. 2014;11(11):1001-1009. doi:10.1002/chem.200400921

142. Carlomagno C, Speranza G, Aswath P, Sorarù GD, Migliaresi C, Maniglio D. Breath figures decorated silica-based ceramic surfaces with tunable geometry from UV cross-linkable polysiloxane precursor. *J Eur Ceram Soc*. October 2017. doi:10.1016/J.JEURCERAMSOC.2017.10.005

143. Maniglio D, Ding Y, Wang L, Migliaresi C. One-step process to create porous structures in cross-linked polymer films via breath-figure formations during in situ cross-linking reactions. *Polymer (Guildf)*. 2011;52(22):5102-5106. doi:10.1016/j.polymer.2011.08.054

144. Stenzel MH, Davis TP. Formation of Honeycomb-Structured, Porous Films via Breath Figures with Different Polymer Architectures. 2006;44:2363-2375. doi:10.1002/pola

145. Wong KH, Davis TP, Barner-kowollik C, Stenzel MH. Honeycomb structured porous films from amphiphilic block copolymers prepared via RAFT polymerization. 2007;48:4950-4965. doi:10.1016/j.polymer.2007.06.048

146. Stenzel MH, Davis TP, Barner-Kowollik C, Davis TP. Formation of Honeycomb-Structured, Porous Films via Breath Figures with Different Polymer Architectures. *J Polym Sci Part A Polym Chem*. 2006;44(8):2363-2375. doi:10.1002/pola

147. Sel O, Laberty-Robert C, Azais T, Sanchez C. Designing meso- and macropore architectures in hybrid organic–inorganic membranes by combining surfactant and breath figure templating (BFT). *Phys Chem Chem Phys*. 2009;11(19):3733. doi:10.1039/b821506e

148. Zhu Z, Reed WF. Enhanced Surfactant Supramicellar Assembly by Hydrophobic Dopants. *Langmuir*. 2013;29(33):10376-10382. doi:10.1021/la402107z

149. Jiang X, Zhang T, Xu L, Wang C, Zhou X, Gu N. Surfactant-Induced Formation of Honeycomb Pattern on Micropipette with Curvature Gradient. *Langmuir*. 2011;27(9):5410-5419. doi:10.1021/la200375t

150.   Wu X, Wang S. Regulating MC3T3-E1 Cells on Deformable Poly(ε-caprolactone) Honeycomb Films Prepared Using a Surfactant-Free Breath Figure Method in a Water-Miscible Solvent. *ACS Appl Mater Interfaces*. 2012;4(9):4966-4975. doi:10.1021/am301334s

151.   Park MS, Kim JK. Breath Figure Patterns Prepared by Spin Coating in a Dry Environment. doi:10.1021/la035915g

152.   Vorotilov K, Petrovsky V, Vasiljev V. Spin coating process of sol-gel silicate films deposition: Effect of spin speed and processing temperature. *J Sol-Gel Sci Technol*. 1995;5(3):173-183. doi:10.1007/BF00487014

153.   Ma H, Kong L, Guo X, Hao J. Dynamic insights into formation of honeycomb structures induced by breath figures. *RSC Adv*. 2011;1(7):1187. doi:10.1039/c1ra00367d

154.   Grossenbacher J, Gullo MR, Dalcanale F, et al. Cytotoxicity evaluation of polymer-derived ceramics for pacemaker electrode applications. *J Biomed Mater Res Part A*. 2015;103(11):3625-3632. doi:10.1002/jbm.a.35477

155.   Soraru GD, Sglavo VM, Vulcan F, Babonneau F. Fabrication and characterization of β-SiAlON components from polymeric precursors. In: *Materials Research Society Symposium Proceedings*. Vol 287. ; 1993.

156.   Narisawa M, Funabiki F, Iwase A, Wakai F, Hosono H. Effects of Atmospheric Composition on the Molecular Structure of Synthesized Silicon Oxycarbides. Besmann T, ed. *J Am Ceram Soc*. 2015;98(10):3373-3380. doi:10.1111/jace.13756

157.   Burns GT, Chandra G. Pyrolysis of Preceramic Polymers in

Ammonia: Preparation of Silicon Nitride Powders. *J Am Ceram Soc*. 1989. doi:10.1111/j.1151-2916.1989.tb06129.x

158. BROW RK, PANTANO CG. Compositionally Dependent Si 2p Binding Energy Shifts in Silicon Oxynitride Thin Films. *J Am Ceram Soc*. 1986;69(4):314-316. doi:10.1111/j.1151-2916.1986.tb04738.x

159. Kubiak KJ, Wilson MCT, Mathia TG, Carval P. Wettability versus roughness of engineering surfaces. *Wear*. 2011;271:523-528. doi:10.1016/j.wear.2010.03.029

160. Buser D, Broggini N, Wieland M, et al. Enhanced Bone Apposition to a Chemically Modified SLA Titanium Surface. *J Dent Res*. 2004;83(7):529-533. doi:10.1177/154405910408300704

161. Curran JM, Chen R, Hunt JA. Controlling the phenotype and function of mesenchymal stem cells in vitro by adhesion to silane-modified clean glass surfaces. *Biomaterials*. 2005;26(34):7057-7067. doi:10.1016/j.biomaterials.2005.05.008

162. McBeath R, Pirone DM, Nelson CM, Bhadriraju K, Chen CS. Cell Shape, Cytoskeletal Tension, and RhoA Regulate Stem Cell Lineage Commitment. *Dev Cell*. 2004;6(4):483-495. doi:10.1016/S1534-5807(04)00075-9

163. Carlomagno C, Motta A, Sorarù GD, Aswath PB, Migliaresi C, Maniglio D. Breath Figures decorated silicon oxinitride ceramic surfaces with controlled Si ions release for enhanced osteoinduction. *J Biomed Mater Res Part B Appl Biomater*. doi:10.1002/jbm.b.34221

164. Alami SM, Gangloff SC, Laurent-Maquin D, Wang Y, Kerdjoudj H. Concise Review: In Vitro Formation of Bone-Like Nodules

Sheds Light on the Application of Stem Cells for Bone Regeneration. doi:10.5966/sctm.2015-0413

165. Kilian KA, Bugarija B, Lahn BT, Mrksich M, Kiessling LL. Geometric cues for directing the differentiation of mesenchymal stem cells. doi:10.1073/pnas.0903269107

166. Kawano T, Sato M, Yabu H, et al. Honeycomb-shaped surface topography induces differentiation of human mesenchymal stem cells (hMSCs): uniform porous polymer scaffolds prepared by the breath figure technique. *Biomater Sci*. 2014;2(1):52-56. doi:10.1039/C3BM60195A

167. Park J, Bauer S, Schlegel KA, Neukam FW, von der Mark K, Schmuki P. TiO $_2$ Nanotube Surfaces: 15 nm-An Optimal Length Scale of Surface Topography for Cell Adhesion and Differentiation. *Small*. 2009;5(6):666-671. doi:10.1002/smll.200801476

168. Dalby MJ, Gadegaard N, Tare R, et al. The control of human mesenchymal cell differentiation using nanoscale symmetry and disorder. *Nat Mater*. 2007;6(12):997-1003. doi:10.1038/nmat2013

169. Biggs MJP, Richards RG, Gadegaard N, Wilkinson CDW, Oreffo ROC, Dalby MJ. The use of nanoscale topography to modulate the dynamics of adhesion formation in primary osteoblasts and ERK/MAPK signalling in STRO-1+ enriched skeletal stem cells. *Biomaterials*. 2009;30(28):5094-5103. doi:10.1016/j.biomaterials.2009.05.049

170. Chang H-I, Wang Y. Cell Responses to Surface and Architecture of Tissue Engineering Scaffolds. In: *Regenerative Medicine and Tissue Engineering - Cells and Biomaterials*. ; 2011:569-588. doi:10.5772/21983

171. Kaitainen S, Mähönen AJ, Lappalainen R, Kröger H, J Lammi M, Qu C. TiO $_2$ coating promotes human mesenchymal stem cell proliferation without the loss of their capacity for chondrogenic differentiation. *Biofabrication*. 2013;5(2):025009. doi:10.1088/1758-5082/5/2/025009

172. Travlos GS. Normal Structure, Function, and Histology of the Bone Marrow. *Toxicol Pathol*. 2006;34:548-565. doi:10.1080/01926230600939856

173. McMurray RJ, Gadegaard N, Tsimbouri PM, et al. Nanoscale surfaces for the long-term maintenance of mesenchymal stem cell phenotype and multipotency. *Nat Mater*. 2011;10(8):637-644. doi:10.1038/nmat3058

174. Obata A, Kasuga T. Stimulation of human mesenchymal stem cells and osteoblasts activities *in vitro* on silicon-releasable scaffolds. *J Biomed Mater Res Part A*. 2009;91A(1):11-17. doi:10.1002/jbm.a.32181

175. Reffitt DM, Ogston N, Jugdaohsingh R, et al. Orthosilicic acid stimulates collagen type 1 synthesis and osteoblastic differentiation in human osteoblast-like cells in vitro. *Bone*. 2003;32(2):127-135. http://www.ncbi.nlm.nih.gov/pubmed/12633784. Accessed January 23, 2018.

Academic Events

Publications:

- **C.Carlomagno**, G.Speranza, P.Aswath, GD.Sorarù, C.Migliaresi, D.Maniglio. Breath Figures decorated Silica-based ceramic surfaces with tunable geometry from UV cross-linkable poysiloxane precursor. *Journal of European Ceramic Society.*
- **C.Carlomagno**, A.Motta, GD. Sorarù, P.Aswath, C.Migliaresi, D.Maniglio. Breath Figures decorated silicon oxinitride ceramic surfaces with controlled Si ions release for enhanced osteoinduction. *Under revision* at Journal of Biomedical Materials Research Part B: Applied Biomaterials.
- JH Park, EY Shin, M. Shin, MJ Choi, **C. Carlomagno**, JE. Song and G Khang. Enhanced retinal pigment epithelium (RPE) regeneration using curcumin/alginate hydrogels: in vitro evaluation. International Journal of Biological Macromolecules.

Congresses:

- **Oral and Poster Presentation** Frontiers on BioPolymers School, Riva del Garda 2015 and 2016
- **Oral Presentation** Bone-Tec, Munich, Germany 2017
- **Oral Presentation** Macrogiovani, Trento 2017
- **Poster Session** Korean Society for Biomaterials, Busan, South Korea 2018
- **Poster Session** biomarkers and biogenesis of extracellular vesicles 2018

- **Poster Session** BioSpine AsiaPacific, Seoul, South Korea 2018

Acknowledgments

First of all, I want to thank prof. Claudio Migliaresi and prof. Devid Maniglio for the support and the mentoring activity during the period at the BioTech Research Center. I'm really grateful also to all the people of BioTech Lab for their support, collaboration and help during these years. In particular I want to thank prof. Antonella Motta, Dr. Water Bonani and Dr. Lorenzo Moschini for their huge support and precious suggestions. I want also to express my gratitude to all the people (colleagues, ex-colleagues, students and friends) that I meet during these years, in particular Dr. Filippo Benetti, Rosa Silvia Raggio, Dr. Nicola Cagol, Silvia Chiera, Francesca Agostinacchio, Luisa Cossu, Dr.Yuejiao Susan Yang, Sofia Santi, Dr. Natascia Cozza, Davide Costantini, Thianjing Zhao, Yu Gu, Peppe, Sim Chen, Motto Raggio, La Lina and all the people from Zorbas. I want also to express my grateful to prof. Gian Domenico Sorarù and Dr. Giorgio Speranza for their huge support for the experimental sessions and data interpretation. I want to express also my gratitude to prof. Aswath Pranesh (University of Texas at Arlington) and prof. Gilson Khang (Chonbuk National University at Jeonju) for their help and support for the beautiful periods spent abroad. I want also to thank Davide, Steven and Francisco for their friendship at the Maverick Place and, in the same way, also to all the people of Gilson's Lab for their huge help with the korean language and with the lab experience. I want also to thank all the people working at LABION for their help and support. I want to express a particular thank to all my friends for sharing with me all my entire life despite the distance.

Obviously, the biggest thank to my family for their continuous and unconditional support during these years...

...and I want to say a particular "thank you Nonna" to my grandmother...probably the best person I have ever met. Everyone should have a person like her in their lives...